PHYSICS-BASED PREDICTIVE TIME PROPAGATION METHOD FOR MONTE CARLO COUPLED DEPLETION SIMULATIONS

A Dissertation

by

JESSE MERLIN JOHNS

Submitted to the Office of Graduate and Professional Studies of
Texas A&M University
in partial fulfillment of the requirements for the degree of

DOCTOR OF PHILOSOPHY

Chair of Committee,	Pavel Tsevtkov
Committee Members,	Les Braby
	Shannon Bragg-Sitton
	Jaakko Leppänen
	Guergana Petrova
	Warren Reece
Head of Department,	Yassin Hassan

December 2014

Major Subject: Nuclear Engineering

ABSTRACT

The Monte Carlo method for solving reactor physics problems is one of the most robust numerical techniques for analyzing a wide variety of systems in the realm of reactor engineering. Monte Carlo simulations sample on fundamental physical processes without making significant numerical approximation while using the best available data describing nuclear interactions with matter. These calculations are often used as benchmarks for faster, lower fidelity deterministic codes. As computing systems become more powerful, the Monte Carlo method has become quite popular and coupling to other methods/codes is almost ubiquitous. A typical coupled calculation might include the assessment of the time dependent behavior of reactor materials resulting from irradiation. The Monte Carlo neutron transport calculation is already a significant computational task; the multiscale depletion simulation significantly increases the computational requirements. This type of coupling is often performed with an operator splitting technique; the neutron transport solution feeding reaction rates to the deterministic depletion simulation. It is shown by manual temporal refinement studies that it is imperative to resolve the change in the neutron flux and cross-sections in time to minimize errors resulting from the temporal discretization. Often in practive, the temporal convergence is checked by running additional simulations with increased time resolution; an often wasteful task if further refinement is not necessary. By assessing driving characteristics of coupled neutron transport and depletion calculations, a new method is developed using a physics-based approximation to predictively adapt the time step, with minimal computational cost, to ensure a close-to-converged coupled simulation. This method develops a temporal grid such that a priori knowledge of time steps is not required

and that further refinement studies become unnecessary. This method was tested with various permutations of light water reactor cases with satisfactory results.

DEDICATION

No matter where I am now, I could never have gotten here without the help of others. I would like to dedicate this to all those that have provided me with a helping hand and showed me kindness along the way. I am greatly indebted to the people that supported me, despite my failings to express how gracious I am for their encouragement.

ACKNOWLEDGEMENTS

I would like to extend my sincerest gratitude to my committee chair, Dr. Tsvetkov, and committee member, Dr. Bragg-Sitton, for providing me with the opportunity and motivation to continue my education. It was through their belief in me and the time they spent guiding my growth that I was able to succeed in the pursuit of this doctorate degree. I would like to thank Dr. Jaakko Leppännen, the developer of Serpent, for all of the stimulating conversations, his extensive coding expertise and insight in extending this method within Serpent. Without his support I would likely not have completed this research in my natural lifetime. I would like to extend a special thank you to Dr. Dan Reece who mentored me throughout my entire existence in the Nuclear Engineering Department. His kindness and advice has been invaluable to me and to my writing. I would also like to thank the rest of my committee, Dr. Braby and Dr. Petrova, for their support. Though my topic has changed a few times, they still provided encouraging support and valuable insight.

I would also like to thank my parents, Marion and Richard Johns, for their ceaseless patience and love. And lastly, I have to thank Lilianna Wolf for being my closest friend, reminding me to eat, and making sure that I live life every once in awhile.

NOMENCLATURE

BOS	Beginning of step
CRAM	Chebyshev Rational Approximation Method
EOS	End of step
MC	Monte Carlo
ODE	Ordinary Differential Equation
PC	Predictor-Corrector
TTA	Transmutation Trajectory Analysis

Symbols

h	Time step size
k	Multiplication factor
p	Time step correction parameter
$\mathbf{r}$	Position vector
t	Time
v	Neutron velocity
$\mathbf{x}$	Solution vector
C	Delayed neutron precursor concentration
C_x	Fitting coefficient
D	Diffusion coefficient
E	Energy
J	Neutron surface current
L	Loss operator

$\mathbf{M}$	Nuclide transmutation operator
$\mathbf{N}$	Nuclide density matrix
N	Nuclide density
P	Production operator
R	Reaction rate
S	Neutron source
V	Volume
∇	Gradient operator

Greek Letters

γ	Fission product yield
ϵ	Error
ν	Neutron yield per fission
λ	Decay constant
σ	Microscopic interaction probability
ϕ	Scalar neutron flux
ψ	Angular neutron flux
χ	Neutron yield energy distribution
Δ	Difference operator
Σ	Macroscopic interaction probability
$\mathbf{\Omega}$	Solid angle of neutron travel

Subscripts

d	Delayed neutron
f	Fission neutron interaction

f	Final time
i, k, m, n	Nuclide index
i	Time step index
j	Interaction type
k	Cell index
p	Prompt neutron
s	Scattering neutron interaction
t	Total neutron interaction
R	Removal neutron interaction
γ	Radioactive capture interaction

Superscripts

q	Level of temporal refinement
C	Corrector step
P	Predictor step

TABLE OF CONTENTS

Page

LIST OF FIGURES

FIGURE Page

1. INTRODUCTION

The use of Monte Carlo (MC) reactor physics codes has proliferated as computing resources become cheaper and more powerful [1, 3, 9, 15, 24, 33]. Their use is expanded by the simplicity and accuracy of their implementation in simulating physical phenomena [16], particularly in the simulation of neutron transport within a nuclear reactor. Such codes are being coupled to include other physical phenomena to approach a more accurate representation of a real reactor system. The neutron transport equations often include coupling to physics that represent, for example, material transmutation, fuel depletion, and thermal and mechanical feedbacks. The coupling can be performed by analyzing individual physical processes separately, often with different numerical tools. This process is called operator splitting and the approach is often favored since different numerical tools are better optimized for solving different physics. In the arena of Monte Carlo simulation, this operator splitting technique is preferred using an explicit approach over implicit approaches, since the simulation process of the neutron transport equation is a heavy computational burden. As computing resources become more powerful, it is natural for human curiosity to push the limits of the available tools. As larger 2D and 3D nuclear reactor systems begin finding their way on computing clusters [22, 21], flaws in the coupling techniques become apparent.

This dissertation is focused on expanding the capabilities of neutron transport and depletion coupled physics calculations by developing a new, physics-based approach for predictively determining time step requirements during depletion coupled simulations. This general approach dynamically assesses the temporal behavior of the reactor system and determines the next time step for ensuring a temporally

converged coupled calculation. Monte Carlo simulations of the neutron transport equation form the basis of this dissertation; however, this method is not exclusive to any single numerical technique.

The time step requirements in producing a solution change dramatically based on the needs of the modeler and on the characteristics of the system. This coupling is considered "tight" if the dependence of a phenomena is highly sensitive to changes within another phenomena. A tight coupling will typically require more temporal refinement in order to resolve the behavior; however, this is often dependent on the numerical methods used (stability) and the fidelity of results required by the designer. For example, pre-conceptual scoping analyses for determining the the estimated lifetime of a fuel loading may take very few time steps (while using a stable predictor-corrector scheme), but the determination of excess reactivity might require ten times the number. The dynamic behavior of installed poisons, reactor transients, or fissile depletion all require varying temporal resolution for accurate modeling. The method developed in this dissertation is applied to high fidelity simulations requiring temporally converged solutions.

This section provides a brief overview of the Monte Carlo method as applied to reactor physics and discusses the methodology of coupling reactor physics calculations to depletion solvers used to model the isotopic constituents of nuclear fuel during irradiation. It is necessary to understand the implications of these techniques associated with neutron transport and depletion coupling and to understand how both the neutron transport simulation and depletion calculation are numerically represented. The advantages and drawbacks of current coupling techniques will be briefly discussed and a case will be made for requiring temporal convergence in the coupled depletion simulations. In section 2, a more detailed analysis on the temporal convergence requirements will be performed and a physics-based method for determining

time steps will be introduced. In section 3, this method is demonstrated using the verification cases from the second section. The method is shown to predictively adapt the time step to ensure an adequately temporally converged neutron transport and depletion simulation.

1.1 Monte Carlo Reactor Physics

Monte Carlo techniques for numerical simulation has humble beginnings during the Manhattan project. They were developed to rein in intractable problems of nuclear implosion hydrodynamics, thermonuclear reactions, and computing neutron fluxes and core criticality. The flight tracks of neutrons were computed via large tracts of paper and an analog computer: the Fermiac [30, 29]. The use of probability sampling to solve simple problems dates back even further to Georges Louis LeClerc, Comte de Buffon in the 1700's [16], but did not come into common practice until digital computers were developed. The modern-day computer can perform Monte Carlo simulations of highly complicated geometries with thousands of nuclides within a matter of seconds to minutes.

Monte Carlo-based reactor physics has a variety of beneficial aspects when applied to general systems. Monte Carlo simulations of neutron transport use a macroscopic, probabilistic description of neutron interactions in the most basic, experimental form. This technique simulates the expected behavior for complex systems by simulating each individual neutron life history within the system and averaging the results. This works well since measuring the macroscopic results of neutron bombardment is relatively simple and more predictable compared to attempting to assess the fundamental nuclear physics of the interactions. This aspect of Monte Carlo simulation has demonstrated itself in supporting basic physics research [2, 8] and by often providing benchmark solutions for other numerical codes.

1.1.1 Neutron Transport

In general, Monte Carlo-based transport simulations simplify the description of problems by sampling the probability density functions representing the physical processes within a system. This is performed by observing the life-history of a single particle within the phase-space of the system. In reactor physics, the numerical modeling of a neutron contains dimensions of space, time, angle, and energy, which can often lead to intractable deterministic numerical solutions unless appropriate approximations are introduced. These approximations typically are system dependent and limit the application of deterministic methods for modeling general reactor systems. The approach to represent the huge dimensional space is greatly simplified in the Monte Carlo simulation; in fact, the spatial, energy, and angle dependencies have infinite resolution using basic physical sampling. The process of sampling the integral form of the neutron transport equation is performed by tracking the behavior of a population of neutrons within the reactor geometry [35]. It should be noted that the MC simulation process does not actually solving the Boltzmann transport equation [24], but rather it is sampling the reaction rate j of nuclide i over a volume V and all incident neutron energy, E:

$$R_{j,i}(\mathbf{r},t) = \int_V \int_0^\infty N_i(\mathbf{r},t)\sigma_{j,i}(E)\phi(\mathbf{r},E)dEdV, \tag{1.1}$$

where $\mathbf{r}$ is a position vector over the geometry, N is the nuclide density, σ is the microscopic cross-section representing the probability of reaction j occurring, and ϕ is the scalar neutron flux, which describes the total length traveled by all neutrons of energy E per unit volume per second. In general, the transport of neutrons can be represented by the Boltzmann transport equation. This transport equations illustrates the dependence of the neutron flux on materials within the reactor geometry.

Therefore, the neutron transport can be described by the time dependent, angular neutron transport equation:

$$\frac{1}{v(E)}\frac{\partial\psi(\mathbf{r},E,\mathbf{\Omega},t)}{\partial t}+\mathbf{\Omega}\cdot\nabla\psi(\mathbf{r},E,\mathbf{\Omega},t)+\Sigma_t(\mathbf{r},E,t)\psi(\mathbf{r},E,\mathbf{\Omega},t)=$$
$$\frac{\chi_p(E)}{4\pi}\int_0^\infty\nu_p(E')\Sigma_f(\mathbf{r},E',t)\phi(\mathbf{r},E',t)dE'+\sum_{j=1}^{N_d}\frac{\chi_d(E)}{4\pi}\lambda_j C_j(\mathbf{r},t)+$$
$$\int_{4\pi}\int_0^\infty\Sigma_s(\mathbf{r},E'\rightarrow E,\mathbf{\Omega}'\rightarrow\mathbf{\Omega},t)\psi(\mathbf{r},E,\mathbf{\Omega}',t)dE'd\mathbf{\Omega}'+S(\mathbf{r},E,\mathbf{\Omega}',t), \tag{1.2}$$

where v is the neutron velocity, $\mathbf{\Omega}$ is the solid angle of neutron travel, χ is the neutron yield for prompt, p, and delayed, d, neutron emission, λ_j is the delayed neutron decay constant for delayed precursor group j, C is the delayed neutron group concentration, S is a source term, and the macroscopic cross-section, Σ_k, is represented by:

$$\Sigma_j(\mathbf{r},E,t)=\sum_i N_i(\mathbf{r},t)\sigma_{j,i}(E), \tag{1.3}$$

where the scalar flux, ϕ, and angular flux, ψ, are related in the following manner:

$$\phi=\int_{4\pi}\psi(\mathbf{\Omega})d\Omega. \tag{1.4}$$

The neutron transport equation can be further simplified by integrating over the angular phase-space, making a diffusion approximation with Fick's Law and forming the equation into a steady-state eigenvalue problem, ignoring delayed neutrons, and by lumping the continuous energy neutron distribution into a multi-group approximation:

$$-\nabla D_g(\mathbf{r})\nabla\phi_g(\mathbf{r}) + \Sigma_{R,g}(\mathbf{r})\phi_g(\mathbf{r}) = \sum_{g'=1}^{G} \Sigma_{s,g'\to g}(\mathbf{r})\phi_{g'}(\mathbf{r}) + \frac{\chi_g}{k}\sum_{g'=1}^{G} \nu_{g'}\Sigma_{f,g'}(\mathbf{r})\phi_{g'}(\mathbf{r}), \tag{1.5}$$

where g is the energy group, G is the total number of energy groups, and D is the diffusion coefficient from Fick's Law :

$$J = -D\frac{\partial\phi}{\partial x}, \tag{1.6}$$

and k is the fission source-forcing eigenvalue or multiplication factor. Σ_R is often called the removal cross-section and is written as:

$$\Sigma_{R,g}(\mathbf{r}) = \Sigma_{t,g}(\mathbf{r}) - \Sigma_{s,g\to g}(\mathbf{r}). \tag{1.7}$$

In other words, the removal cross-section is the total cross-section without in-group scattering (scattering that doesn't result in the neutron changing energy). The neutron diffusion equation can be further simplified by discretization in energy and reducing to a matrix-operator notation:

$$[L - \frac{1}{k}P - S]\phi = 0, \tag{1.8}$$

where L is the loss operator formed by the left-hand of equation 1.5. P is production operator and S is the scattering operator formed by the right-hand side of equation 1.5. In solving this system, the following condition needs to be true for a non-trivial solution to exist:

$$k = (L + S)^{-1} P, \tag{1.9}$$

where the operators L, S and P can be directly sampled in the MC simulation. This lends itself to a simplistic approach for MC calculations of the multiplication factor.

When representing the cross-sections, MC codes often use continuous energy cross-section data, which represent the best available information on the interactions of neutrons with matter. These libraries are provided through extensive collaboration and international effort, such as the JEFF [34] and ENDF [7] libraries, for more than 400 nuclides. The deterministic neutron transport code typically use collapsed energy grouped cross-sections to perform faster computations of the transport equation. These collapsed nuclear cross-sections assume weighting based on the neutron energy spectra of the modeled systems. This makes the communicable nature of pre-processed cross-sections, for direct numerical codes, a limitation of their applicability to general reactor analysis.

1.1.2 Law of Large Numbers

This dissertation does not focus on the implications of numerical convergence of the transport solution; however, it is necessary to refresh the discussion, since the assessment of any reactor simulation via Monte Carlo is limited by a defined set of principles. The results of a simulation are based on the sampling of neutron tracks and interactions over some geometry. The sampling accuracy is subject to the total number of neutron histories that are tracked, which follows from the "law of large numbers". This states:

$$\bar{X}_n = \frac{1}{n} \sum_{i}^{n} X_i \rightarrow \mu \text{ as } n \rightarrow \infty, \tag{1.10}$$

where $\bar{X}$ is the average value after n samples, X is the instantaneous value, and μ is the expected value. This essentially states that as the number of samples goes to infinity, the average value approaches the expected value.

It follows from the "law of large numbers" that the errors from sampling are proportional to the neutron density or collision rate density, meaning that the number of samples is greater where the neutron population is larger. The errors on the power profile and fission rate density over the system, in this study, are proportional to the neutron density. This results in poor sampling (and numerical errors) in regions where neutron tracks are an infrequent occurrence. While many codes have variance reduction techniques to reduce these errors, Serpent is quite limited in its features [26]. It was developed primarily for 2D lattice calculations where neutron distributions are expected to be flat, so such variance reduction is an unnecessary development expenditure. However, with the expansion of Serpent 2 for modeling larger systems with significant spatial gradients, a uniform fission source method [22] has been implemented.

The Monte Carlo method is used for computing the neutron flux distribution over the reactor core. It is required that the sampling be sufficient so that the numerical errors are minimized between identical simulations, which can be checked by using different seeds for the random number generator. The numerical error influences the reaction rate density, which results in errors within the depletion solver. These errors can carry through multiple transport and depletion solutions. This can result in divergent results for some numerical schemes.

1.1.3 Serpent 2, Continuous-energy Monte Carlo Reactor Physics Code

Many Monte Carlo codes are available for modeling neutron transport. These come in open-source [1, 33] and government sponsored [3] versions. The code se-

lected for use in developing the temporal convergence method is the Serpent three-dimensional continuous-energy Monte Carlo reactor physics code. Serpent is a relatively new code that has performed remarkably well for reactor calculations [24]. It was originally developed to perform multi-group cross-section collapse, but as the user base expanded, it quickly grew into a general reactor analysis and depletion code. The code continues to be developed at VTT Technical Research Centre in Finland with Dr. Jaakko Leppänen as the main developer of the software.

Serpent 2 is the successor and is currently slated for public release in 2015. Access to the beta code provides an ideal platform in which to implement the developed method. The choice to use Serpent 2, however, is not solely due to the accessibility of the code, but because of its excellent performance in performing large reactor core burnup simulations. The code has been optimized for reactor calculations by taking advantage of relatively flat neutron distributions that are expected in infinite lattice calculations. Serpent employs a few techniques that enhance the speed at which results are obtained via the MC approach. Instead of tracking individual particles through a geometry, the Serpent code applies a so-called "majorant" cross-section over the universe with a method called Delta Tracking [25]. Particle travel is sampled by "virtual" collisions in the entire geometry and specific reactions are sampled at the "virtual" collision sites. This technique avoids the costly track-length estimation since the distance to surfaces are no longer computed. Serpent does retain the surface tracking feature in cases where the efficiency of rejection sampling is poor [25], such as in vacuum or control rod locations. Serpent makes use of a unified energy grid structure for storing cross-sections, reducing the need for table lookups, therefore further enhancing the computational efficiency and speed. This technique is particularly useful when there are a large number of nuclides tracked during burnup simulations.

1.2 Nuclear Fuel Depletion

As nuclear fuel undergoes neutron irradiation, material constituents change due to neutron capture, fission-product production, and decay. The short and long term impact of reactor fuel composition changes can affect the neutron transport behavior. The nuclear designer must account for the loss of fissile material and the production of other nuclides in order to predict reactor behavior and accommodate economic and safety design decisions accordingly.

Depletion simulations are necessary in order to resolve the reactor behavior during operation. Significant changes can occur in the fuel and other materials within the reactor. The reactor designer must have a computational tool to assess design decisions and to anticipate reactor parameters with time. Such an analysis might require the designer to determine if the reactor will operate for the required cycle length or determine, more accurately, the core reactivity with time, resulting from fission product poisons and external thermal responses. This also allows the designer to address control requirements for startup and shutdown, both planned and emergency. There are other designer requirements, related to nuclear fuel burnup, for regulatory needs. These include radiological toxicity associated with various fission product and transuranic concentrations, reactivity and feedback parameters, fission gas buildup, and fuel pin burnup and swelling.

The purpose of the depletion solver is to resolve the atomic density $N_i(\mathbf{r}, t)$ for any nuclide i with time. The mechanisms of transmuting i into any other nuclide are:

$$\frac{dN_i^{decay}(\mathbf{r},t)}{dt} = -\lambda_i N_i(\mathbf{r},t) \tag{1.11}$$

$$\frac{dN_i^{abs}(\mathbf{r},t)}{dt} = -\int_0^\infty \sigma_{a,i}(E)\phi(\mathbf{r},E,t)dEN_i(\mathbf{r},t), \tag{1.12}$$

where λ is the decay constant and the mechanisms for transmuting nuclide k, m, n into i are:

$$\frac{dN_i^{fission}(\mathbf{r},t)}{dt} = \sum_{k\neq i}\int_0^\infty \gamma_i\sigma_{f,k}(E)\phi(\mathbf{r},E,t)dEN_k(\mathbf{r},t) \tag{1.13}$$

$$\frac{dN_i^{capture}(\mathbf{r},t)}{dt} = \sum_{m\neq i}\int_0^\infty \sigma_{\gamma,m\to i}(E)dE\phi(\mathbf{r},E,t)dEN_m(\mathbf{r},t) \tag{1.14}$$

$$\frac{dN_i^{decay}(\mathbf{r},t)}{dt} = \sum_{n\neq i}\lambda_{n\to i}N_n(\mathbf{r},t), \tag{1.15}$$

where γ is the yield of nuclide i from fission. The total rate of change of nuclide i is the sum of all the mechanisms. The result is an ordinary differential system, often called the Batemann equations, and can be solved by numerous methods [18]. One of the approximations often made in this system of equations is that the flux, ϕ, is invariant. In the constant flux case, the solution to the Batemann equations is simple and can be solved with a variety of methods. In particular, Serpent makes use of the Transmutation Trajectory Analysis (TTA) and Chebyshev Rational Approximation Method (CRAM) numerical techniques [32, 27]. The TTA method is based on an analytical solution to the linearized transmutation chain [6] and CRAM solves the matrix form of the depletion equations, which is described more simply:

$$\frac{d\mathbf{N}(\mathbf{r},t)}{dt} = \mathbf{M}(\phi)\mathbf{N}(\mathbf{r},t), \tag{1.16}$$

where $\mathbf{M}(\phi)$ is the matrix operator which contains the physical information from the Batemann equations. In the Monte Carlo calculation, the nuclide density is typically represented as a per-cell quantity, where a cell is the geometric representation of a material within the computational domain. The number of unknowns increases proportionally with the number of cells and nuclides per cell. This can quickly become intractable for modest computing system.

The solution to the depletion equation is not so easy to obtain, however, when the flux is not constant. The system now behaves non-linearly and the set of depletion and neutron transport equations must be solved iteratively. In various deterministic codes, the ordinary differential equation (ODE) set can be solved through the use of methods such as Runge-Kutta while iterating on the neutron flux solution [28]. This implicit coupling comes with a significant computational cost, compensated by the added stability and accuracy in computing the solution. The high computational cost of an implicit method can be avoided by trading off accuracy and using shorter time-steps with an explicit predictor-corrector method. The predictor-corrector method, for neutron transport and depletion coupled simulations, makes the assumption that the neutron flux is constant during the time step and uses a correction step to "correct" the constant approximation. Furthermore, the constant approximation results in a predictor-corrector scheme that is typically conditionally stable and requires some control of the time step interval. This time interval is usually selected by the code user and may or may not be valid. A stable solution, however, does not necessarily result in a correct solution. This requires a temporal convergence study by increasing the refinement in time and assessing the error of the old solution with the new, more refined, solution. This is discussed in the following sections.

In the depletion calculation, the distinction between the transmutation and depletion of materials is explicit. For brevity, however, in this dissertation the term

"depletion" will be used when addressing all of the mechanisms of nuclide production and destruction.

1.3 Monte Carlo Reactor Physics and Depletion Coupling

The neutron transport solution, using Monte Carlo numerical techniques, is solved by sampling a steady state geometry and nuclide inventory. This results in a steady-state solution for the fundamental mode, neutron flux distribution and reaction rate density over the reactor volume. The atomic densities within the system change with respect to time as a result of neutron interactions with matter. This requires a coupling between the neutron transport and depletion solvers over a spatial and temporal grid. Since the depletion, with constant flux, can be solved within machine precision, the error associated with coupling resides in time discretization and reaction rate convergence between the depletion and neutron transport solutions. The two solutions, which depend on each other, need to be updated appropriately in order to ensure that the temporal behavior of the physics is physically represented. This means that the time step should be small enough that the constant approximation is valid or that the correction is performed such that the average behavior of the physics is captured during that time step.

Coupled Monte Carlo and depletion simulations are not a recent development; however, interest in the techniques of coupling has increased as resources sufficient for large-scale coupled calculations have reached researchers. This has resulted in significant development in coupling schemes, particularly with predictor-corrector methods. These methods make predictions on the nuclide inventory at the end of step (EOS) based on the beginning of step (BOS) neutron transport solution. This prediction is corrected by performing another neutron transport simulation with the predicted atom densities and making an informed interpolation on the resulting

solutions. There are many interpolation methods that have been implemented in Serpent 2 [18]; however, the focus here will be on the basic mid-point predictor-corrector scheme, introduced in the next section.

1.3.1 Coupling Strategies

The coupling between the neutron transport and depletion solvers is performed using an operator splitting integration technique, called the predictor-corrector method. The Monte Carlo simulation solves for the neutron flux distribution, $\phi(\mathbf{r}, t)$, assuming constant material properties. During some irradiation interval Δt, the flux $\phi(\mathbf{r}, t)$, is assumed constant:

$$\phi(\mathbf{r}, t_f) = \phi(\mathbf{r}, t) = \phi(\mathbf{r}, t_o), \;\; t \in \Re \mid t_o < t < t_o + \Delta t \tag{1.17}$$

The reaction rates are determined with equation 1.1, and at end of irradiation time, $t_f = t_o + \Delta t$, the atomic density is solved with equation 1.16. The neutron flux is dependent on the atomic density (equation 1.8) so it is expected that the assumption made in equation 1.17 is not strictly valid except for infinitesimal irradiation intervals. Taking extremely small steps is not computationally feasible for large systems. Conversely, small time steps will propagate statistical errors accumulated within the neutron transport solution [10], which can be further exacerbated by some coupling schemes. There have been various coupling schemes developed to address these issues [18] while maintaining a constant flux approximation and allowing the use of larger time steps while maintaining solution accuracy.

Before coming to an example of these methods, the most basic coupling strategy is introduced: the explicit Euler approach. The neutron transport is solved with the BOS atomic density, $N(\mathbf{r}, t_i)$, to find the BOS neutron flux, $\phi^P(\mathbf{r}, t_i)$. The EOS atomic density, $N^P(\mathbf{r}, t_{i+1})$, is solved with Eq. 1.16 from time t_i to t_{i+1}. This method

has poor performance when the time step is large, so a corrector calculation is usually performed.

The mid-point corrector scheme solves for the EOS neutron flux, $\phi^C(\mathbf{r}, t_{i+1})$, using the predicted atomic densities, $N^P(\mathbf{r}, t_{i+1})$, and recomputes the depletion from t_i to t_{i+1}. The resulting EOS atomic density can be computed with a variety of strategies. One such method is to compute the corrected atomic density $N^C(\mathbf{r}, t_{i+1})$. The temporal change in neutron flux is "canceled out" over the time interval by calculating the "final" EOS atomic density as:

$$N(\mathbf{r}, t_{i+1}) = \frac{1}{2}\left(N^P(\mathbf{r}, t_{i+1}) + N^C(\mathbf{r}, t_{i+1})\right) \tag{1.18}$$

The methodology can be better visualized in the following pseudo-code:

for $i := 0$ to N_{steps} do

solveNeutronTransport(N_{BOS})	output: $\phi^P(\mathbf{r}, t_i)$
solveMatrixDepletion($\phi^P(\mathbf{r}, t_i), N_{BOS}$)	output: $N^P(\mathbf{r}, t_{i+1})$
solveNeutronTransport($N^P(\mathbf{r}, t_{i+1})$)	output: $\phi^C(\mathbf{r}, t_{i+1})$
solveMatrixDepletion($\phi^C(\mathbf{r}, t_{i+1}), N_{BOS}$)	output: $N^C(\mathbf{r}, t_{i+1})$
updateAtomicDensity($N_{BOS}, N^P(\mathbf{r}, t_{i+1})$)	output: $N(\mathbf{r}, t_{i+1})$

end

where N_{steps} is the number of total time steps. This pseudo code is over simplified, of course, simply to illustrate the major steps of the coupling process. Other steps, like computing flux-weighted transmutation cross-sections for the depletion matrix are required but not shown. Another method is to use the average neutron flux between the predictor and corrector transport simulations:

$$\phi(\mathbf{r}, t_{i+1/2}) = \frac{1}{2}\left(\phi^P(\mathbf{r}, t_i) + \phi^C(\mathbf{r}, t_{i+1})\right) \tag{1.19}$$

then performs the depletion with the interpolated flux. This is the methodology used in Serpent and can be visualized in the following pseudo-code:

for $i := 0$ to N_{steps} do

solveNeutronTransport(N_{BOS})	output: $\phi^P(\mathbf{r}, t_i)$
solveMatrixDepletion($\phi^P(\mathbf{r}, t_i), N_{BOS}$)	output: $N^P(\mathbf{r}, t_{i+1})$
solveNeutronTransport($N^P(\mathbf{r}, t_{i+1})$)	output: $\phi^C(\mathbf{r}, t_{i+1})$
interpolateFlux($\phi^P(\mathbf{r}, t_i), \phi^C(\mathbf{r}, t_{i+1})$)	output: $\phi(\mathbf{r}, t_{i+1/2})$
solveMatrixDepletion($\phi(\mathbf{r}, t_{i+1/2}), N_{BOS}$)	output: $N(\mathbf{r}, t_{i+1})$

end

The consequence of using the mid-point method is that the number of transport calculations increases by a factor of two. This overall increase in the computation time of the neutron distribution, however, is often off set by an overall increase in the size of the time step. The increase in time step size is often greater by an order of magnitude when using the mid-point method. There are more advanced interpolation schemes that reduce the number of time steps even further; however, to stay with conventional practice, the basic mid-point PC method is used for the rest of the dissertation.

1.3.2 Spatial Stability

Stability issues can arise as a result of the operator-split coupling scheme [10, 12]. The stability is a strong function of the statistical convergence and the tightness of coupling between the depletion solver and the neutron transport calculation. In

the stochastic Monte Carlo simulation, the neutron transport process is simulated similarly to the real physical process. This leads to a pseudo-physical/numerical noise that can be amplified if the simulation is not appropriately converged, if the coupling scheme is crude, and/or if the system being modeled is large compared to the neutron mean-free path length. This is physically observed in end-of-life reactor cores which are loosely coupled, in the form of Xe-oscillations, but can also be observed nonphysically as a result of numerically related phenomena.

Spatial instability can also be onset by spatial non-uniformity resulting from external variations. One such example of such a case results from axial temperature variations resulting from the enthalpy increase of coolant passing along the length of a fuel rod and the coupling of the neutron transport simulation to such thermal-hydraulic responses [23].

The method developed in this dissertation will be focused on 2D geometries without coupling to physics other than nuclear fuel depletion for these reasons. Infinite-lattice cases minimize spatial stability concerns from the method development.

1.4 Temporal Convergence

The focus of this dissertation is the method development to predictively determine the required number and size of time steps for a converged neutron transport and depletion coupled simulation. This method dynamically assesses the behavior of the reactor system and selects the next burnup time step during the depletion simulation. The importance of selecting appropriate time steps with the predictor-corrector method outlined above is a result of the simulation dependence on the temporal resolution. This is a consequence of the explicit predictor-corrector methods. The use of PC methods can reduce the computational effort of performing neutron transport simulations at the cost of requiring more resolution in time com-

pared to implicit methods. The impact of temporal resolution is investigated before the adaptive time-step method is developed.

The term temporal convergence, strictly speaking, is such that the following criteria is met:

$$\epsilon = \max(|\mathbf{x}^{q+1} - \mathbf{x}^{q}|) \leq \epsilon_{\text{tol}} \tag{1.20}$$

where $\mathbf{x}$ is a solution vector, q and $q+1$ represents the levels of temporal refinement, and ϵ_{tol} is the error tolerance. In this formation, the comparison between solutions only occurs for times of the lower level of refinement. The error tolerance is selected to meet various criteria: for the eigenvalue is set to 10 pcm and for atom densities it is set to 5 % on the relative difference. These selections are based on the study in section 2. The statistical error is reduced significantly below these tolerances to prevent the temporal convergence from being stochastic; fluctuations resulting from the Monte Carlo method will not influence the temporal resolution.

1.4.1 Takahama-3 NEA Benchmark

A 2D, infinite lattice calculation of a square, light water reactor (LWR) type lattice is used for this analysis, as it is one of the most studied reactor physics problems. The Takahama-3 NEA Benchmark [31, 17] was selected to fit this criteria. The geometric, material and power history parameters can be found in the references.

The selection of an infinite lattice calculation introduces some limitations for the development of this methodology. The predominate simplification comes from the relatively flat flux profile over the lattice resulting from the periodic boundary conditions and long mean-free path relative to the fuel pin diameter. The reaction rate gradients can be rather steep in regions with burnable poisons, such as in this benchmark. Consequently, the time-step, adaptive method will likely be limited to

the infinite lattice calculation; it is expected that the large spatial gradients in the flux over full-core geometries will introduce more degrees of freedom which are not addressed in this dissertation.

Despite its simplicity, the LWR lattice provides a few benefits over other reactor configurations. Large spatial gradients in the reaction rate are expected owing to the strong self-shielding that occurs in fuel pins and particularly in the burnable absorbers. These strong gradients introduce significant temporal convergence requirements for capturing the coupled behavior. These requirements, specifically, will be addressed in Chapter 2. Another advantage of the LWR system, for this analysis, is that reactor behavior is very sensitive to the material density and its constituents, providing that a robust methodology can be derived for this configuration and may be applicable, with minor adjustment, to other systems. This expansion to other reactor systems will not be the focus of this dissertation. Lastly, the LWR configuration probably constitutes the most stylish nuclear engineering study problem resulting from its wide use as the premiere nuclear power reactor design in the United States. This a priori knowledge of LWR behavior lends itself to assisting conceptual and computational analysis.

When committing oneself to performing a neutron simulation with the MC method, the first step is to ensure numerical convergence by simulating the appropriate number of histories. Since the MC simulation obeys the Law of Large Numbers, only a few simulations are required to extrapolate the number of histories that need to be simulated to ensure the relative errors on fuel pins are small. Figure 1.1 shows the results of a numerical convergence study on the eigenvalue with burnup, where the legend indicates the total number of neutron histories simulated per depletion step. This plot is generated by performing eight separate simulations with different starting random seeds; the results are averaged with the standard deviation computed

assuming a normal distribution. These are shown as a function of time so that the depletion steps when reactor power is zero can be seen. With poor statistical convergence, the final solution converges to the expected value when results are averaged over a few batched simulations produced from different random seeds. This is the result of the so-called "cancellation of error" which arises as a result of oscillations in the spatial reaction rates [10]. In other words, a significant divergence from the mean is not expected; however, at any single time step, the standard deviation may be unacceptable for reactor analysis, precluding the need for a numerically converged simulation.

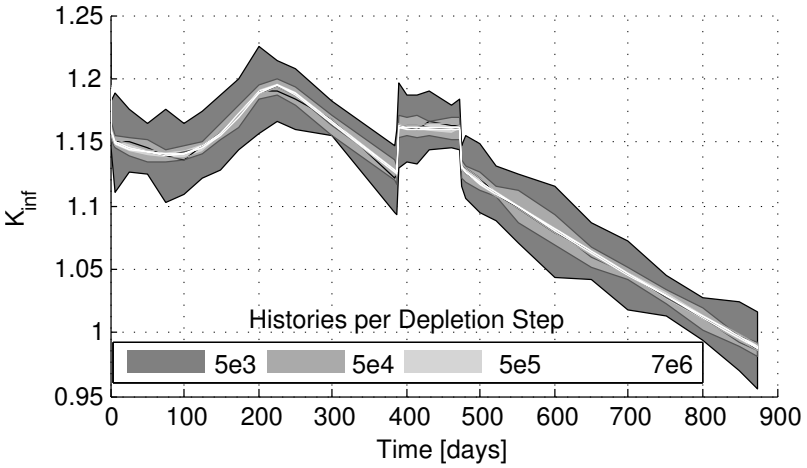

Figure 1.1: Statistical convergence of eigenvalue value.

Figure 1.2 shows the impact of numerical convergence on a few select important nuclides with burnup. These plots are generated in the same fashion as figure 1.1. The error resulting from poor statistical convergence can be rather significant for short-lived nuclides; however, the expected value is usually achieved when many

simulations are averaged. Again, this result suggests that there is no significant divergence in the computed value with poor statistics.

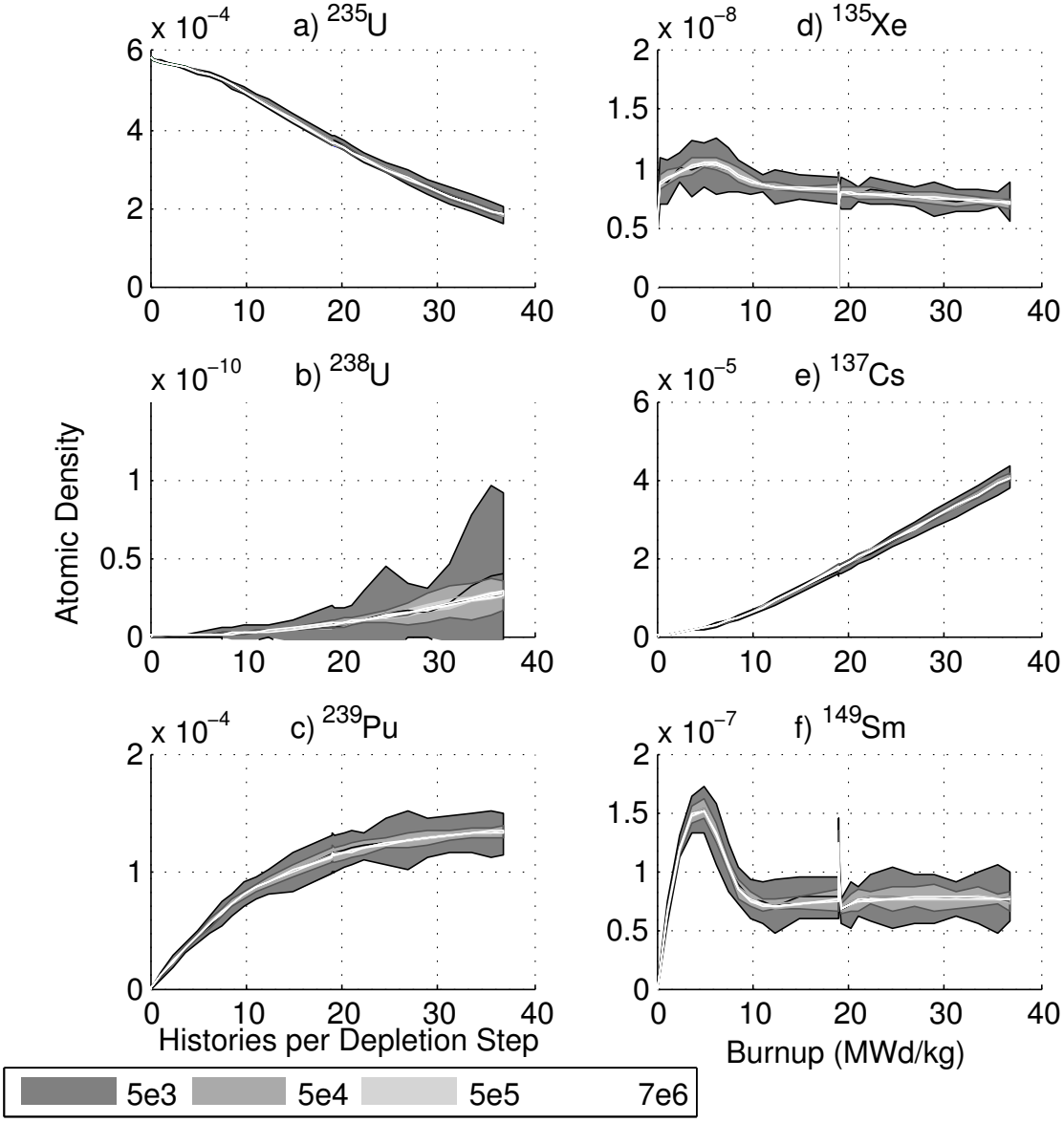

Figure 1.2: Statistical convergence of atomic density for select nuclides in UO_2/Gd_2O_3 fuel pin.

The statistical convergence is an important source of error in the simulation

process. This is not a major focus point of this dissertation. There are a vast number of other influences on the accuracy of the burnup simulation; however, the most significant influence results from temporal convergence considerations.

The number of time steps required in a lattice simulation is dependent on the numerical treatment (for example the PC method used) and the tightness of coupling between the depletion and neutron transport solutions. The Takahama-3 benchmark is expected to have tight coupling since the lattice contains burnable absorber rods. More temporal resolution is required during the Gd depletion, resulting from the flux distribution changing shape and magnitude in these localized regions. Figure 1.3 shows the results on the eigenvalue by incrementally increasing the number of time steps. This figure shows the temporal convergence of the infinite multiplication factor (top) as a function of burnup, where the legend indicates the number of time steps for each of the simulations. A manual adaptivity was used by adding a time step where the difference in the multiplication factor (bottom) was larger than 10 pcm. A converged solution was obtained for the multiplication factor.

The error in the eigenvalue is reduced as the time step size is refined. The largest error, and therefore the most temporally refined portion of the coupled depletion simulation is seen at a burnup of $10 - 12\frac{MWd}{kg}$. This corresponds to when the depletion of the Gd in the burnable absorber rod is completed to a level where the Gd cross-section's influence on the neutron transport solution is becoming negligible. This results from the significant change in the spatial gradient of the reaction rates, particularly because the depletion of the Gd is localized. On the other hand, the burn-in of fission products at a burnup of $< 0.5\frac{MWd}{kg}$ is nearly evenly distributed, since it is proportional to the fission rate density and reaches equilibrium quickly.

Figure 1.4 shows the impact of the temporal convergence on the reaction rates over the lattice. This figure shows the difference in the flux (a) and the reaction

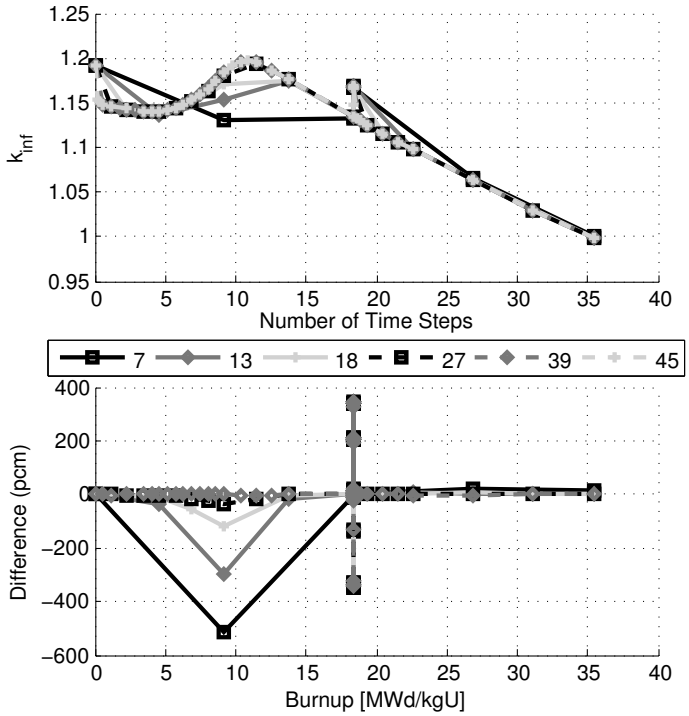

Figure 1.3: Temporal convergence of the infinite multiplication factor (top) and relative difference in the multiplication factor (bottom).

rates (b) of a temporally converged mesh (c) with 39 time steps (shown in Figure 1.3) to a case with only 7 time steps (d) at a burnup of 9.16 $\frac{MWd}{kg}$ for a 1/4 of a PWR assembly.

The differences in the reaction rate are most significant in the burnable absorber pins. This further illustrates why the result in figure 1.3 requires many time steps to resolve. The depletion rate of the Gd changes the flux significantly in these localized regions. This spatial and temporal change in the flux distribution is not resolved with the large time steps.

Figure 1.5 shows the impact of temporal convergence on select nuclides. There is a large discrepancy in the computed burnup within the pin, after 385 days of irradiation. The burnup in the pin of interest is 11.53 $\frac{MWd}{kg}$ for the resolved case

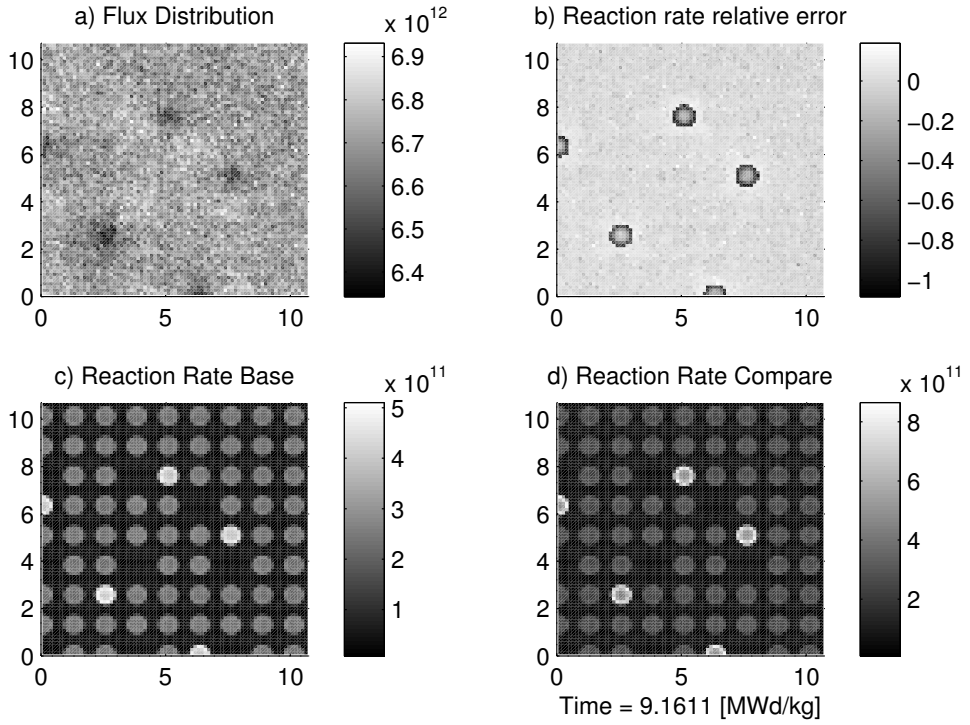

Figure 1.4: Quarter assembly relative flux and reaction rates.

for 45 time steps and 8.12 $\frac{MWd}{kg}$ for the case with the fewest number of time steps, representing a 30 % relative error. The atom densities converge after about 20 $\frac{MWd}{kg}$; however, the transient behavior during the Gd depletion is not resolved until 39 times steps are used.

1.4.2 Further Discussion

The results of this short, qualitative study demonstrate the need for proper time stepping when solving neutron-depletion coupled simulations. This behavior is often accounted for in many burnup studies [5, 36], however, the basis for adjusting the number and size of time steps usually results from the experience of the user in solving these types of problems. In other words, there is no current standard for a

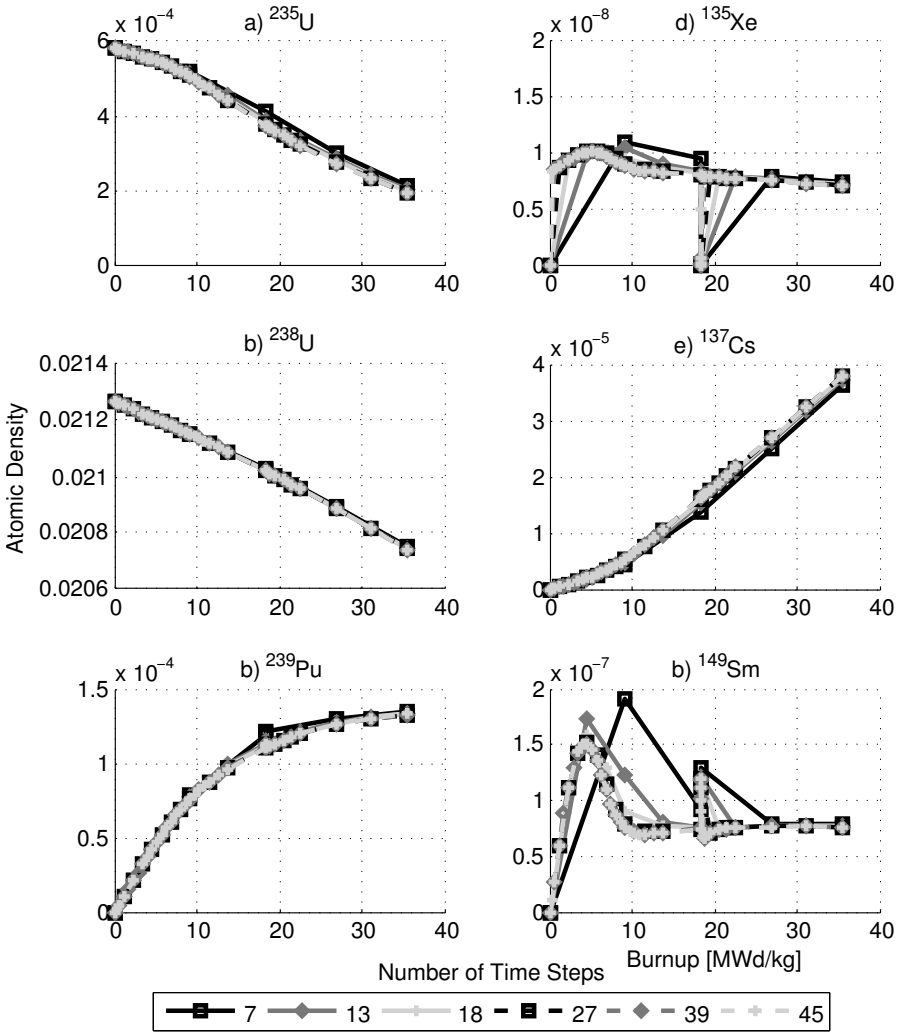

Figure 1.5: Temporal convergence of atomic density for select nuclides in UO_2/Gd_2O_3 fuel pin.

vigorous approach in selecting proper time steps or for performing burnup refinement studies. Only recently has the temporal convergence issue been reviewed in literature [13] for reactor simulations.

The progress and development in Monte Carlo-depletion coupling has demonstrated issues resulting from the conditionally stable methods used in Monte Carlo codes to date where fully-implicit methods are computationally impractical. There

have been studies that investigate advanced PC methods to allow for longer time steps [19, 23] and improve numerical stability [11]. In effect, they have exposed spatial and numerical stability issues, which often arise from perturbations in the system resulting from various phenomena. These can range from numerical to physical. For example, if the stochastic errors are larger than systematic errors, the simulation can exhibit nonphysical oscillations between the neutron transport and depletion calculations. Additionally, real, physical behavior can introduce the same oscillations, as demonstrated in reference [23].

This study also illustrates that the temporal requirements for a depletion simulation are extremely important when attempting to simulate depletion-dependent reactor behavior. Temporal requirements for depletion simulations have received little attention compared to statistical analyses [36, 14, 4]. Comparing figures 1.2 and 1.5, one might conclude that time stepping is quite an important concern that has been understudied. Addressing these concerns is a focus of this dissertation.

1.5 Objectives

The objective of this dissertation is to develop a physics-based approach to predictively determine the time steps necessary to ensure a close-to-converged simulation for light water reactor systems. The developed method is performed dynamically during the coupled simulation. Specifically, it is performed at the predictor step to reduce computational requirements. This method is a novel first-approach to this temporal convergence problem and is not limited to Monte Carlo reactor physics codes.

2. PREDICTION OF TIME STEP DISCRETIZATION

The evidence provided demonstrates that the reactor designer must depend on prior knowledge when solving a coupled neutron transport and depletion calculation. The selection of time steps depend heavily on the physical parameters of the system being modeled. Significant refinement in time is required to resolve the reaction rate and isotopic densities spatially and temporally. This necessitates a temporal convergence study to ensure that the time-dependent behavior is fully resolved. This kind of study, however, can be unnecessarily expensive, requiring a second, exclusive simulation to be re-run with a greater number of time steps.

The prior knowledge for time step selection derives from experience in solving these problems, and therefore can be problematic if the code user does not perform a temporal convergence study when expanding beyond the user's experience. The most prominent example is the analysis of assemblies with installed burnable poisons. It is shown later that fidelity requirements of the simulation do depend on the results that the code user desires. This section discusses the development of a general method to dynamically determine the time step requirements in order to satisfy the temporal discretization requirements for a temporally converged solution.

The following outlines a method that can provide a physics-based approach to solve this problem and automatically determine the necessary time steps for a close-to-converged neutron transport and depletion coupled simulation. This section will start by addressing the temporal requirements needed for a variety of cases. Once time step needs are established, a method is outlined which provides reasonable estimations for the time step requirements. In the next section, this method will be demonstrated.

2.1 Temporal Convergence Requirements

In this section, the requirements for producing a temporally converged solution for the Monte-Carlo neutron transport and depletion coupled simulation will be addressed. A variety of permutations of the LWR lattice are considered. These include the following:

- Standard 17x17 lattice without burnable absorbers.
- Standard 17x17 lattice with burnable absorbers.
- Standard 17x17 lattice with burnable absorbers and spatial discretization.
- Reduced 3x3 lattice with burnable absorbers and spatial discretization.

The aforementioned cases were selected to isolate different phenomena which contribute to the temporal discretization needs, including the initial burn-in of fission products and the depletion of installed burnable and fissile material. In addition, it is important to address self-shielding and assess the impact of systems where the depletion of burnable absorbers dominate system behavior. The spatial discretization of the burnable absorbers will not be exhaustive in order to maintain reasonable computational requirements. Further studies on the statistical convergence are necessary with an increase in the number of burnable materials, as is the case with increasing the spatial resolution. In additional, the number of neutron histories will have to increase to accomodate the additional zones which must be sampled. It is not necessary to perform very detailed spatial resolution studies for this research.

In the following studies, the application of temporal refinement is performed adaptively. Uniform refinement is not desirable since it can be computationally wasteful, as will be seen. The adaptivity is performed by assessing the error on the

eigenvalue, nuclide densities, and reaction rates for each global time step and refining the previous time steps. Since the burnup is explicit in time, it is natural that errors from the initial coarse resolution will be propagated forward in time. There types of errors are called systematic errors. A uniform step size of 4 $\frac{MWd}{kg}$ will be used for the initial refinement level; each further level of refinement will be performed incrementally from time zero forward.

The burnable absorber rods are spatially discretized, unless otherwise noted. This discretization is performed in order capture predominate self-shielding effects in the lattice. Fuel regions without burnable poisons are not discretized. The spatial discretization of the burnable absorber rods is not exhaustive to ensure timely computations in converging the reaction rates in these zones. As more cells are added the number of neutron histories increase to ensure local, statistical convergence in the reaction rates. There is a trade-off for computational speed and accuracy. It is necessary to capture this effect in order to establish proper treatment in this study; however, a fully spatially "real" analysis introduces no added benefit to this research.

2.1.1 Standard 17x17 lattice without burnable absorbers

The first case to be analyzed is the standard 17x17 LWR infinite lattice without burnable absorbers, shown in figure 2.1. The dimensions and materials are identical to those used in the NEA benchmark [31, 17]. Nuclide densities are tracked for the location that is equivalent to the SF95 position in the benchmark.

The calculation of multiplication factor as a function of burnup is shown in figure 2.2 for each level of refinement on the left and with the error in pcm for each added level of refinement on the right, where the legend indicates the number of time steps. The refinement in this case is heavily dominated by converging the nuclide distribution (see figure 2.3) rather than the reaction rate. More temporal refinement

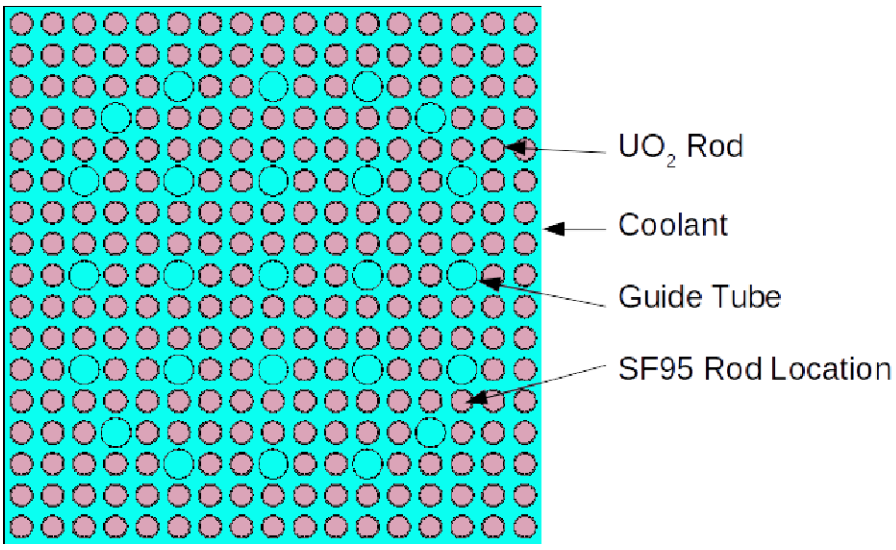

Figure 2.1: Geometry of 17x17 LWR lattice without burnable absorber rods.

is required and results from the time dependence of the decay modes of radionuclides which have a significant impact on the neutron transport solution. In other words this results from the coupling of the depletion and neutron transport solution. These time constants, discussed later, limit the time step size in the non-equilibrium regions. The time steps used in this case and all of the following cases will be shown in the final discussion to reduce redundancy.

This figure also demonstrates that the convergence of the infinite multiplication factor is quite rapid when there are no BAs in the fuel assembly, comparing to the results in the previous section. The reaction rate distribution is fairly flat, as shown in figure 2.4, and overall, the most significant errors come from the statistical convergence for this case.

In figure 2.3, the nuclide concentration in the SF95 rod is shown for a few select nuclides at each level of refinement on the left. The concentrations are normalized to the maximum value of the most refined case. Also shown in this figure are the

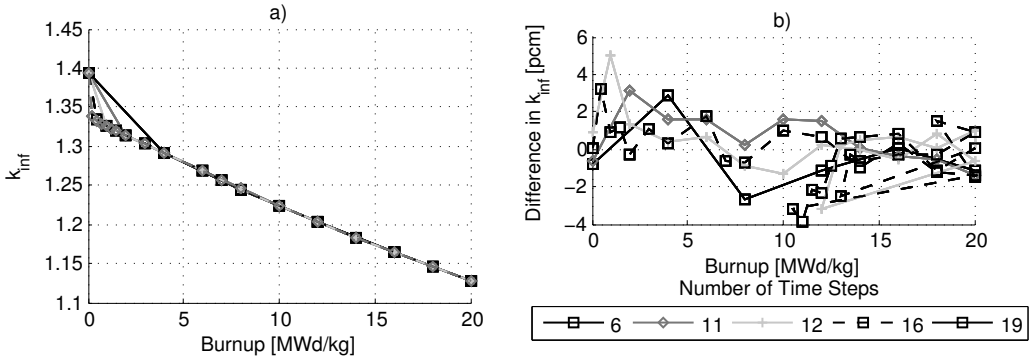

Figure 2.2: Infinite multiplication factor of 17x17 LWR lattice without burnable absorber rods.

relative errors for each selected nuclide on the right. Systematic error is evident in all of the nuclides. The errors for nuclides that have a zero concentration in the fuel, near the beginning of life, result from very low concentrations that are very sensitive to the temporal solution. These errors, however, are very small and the resulting propagation of error is minimal.

In using the convenient unit of burnup, $\frac{MWd}{kg}$, as a time step, there is an implicit error that arises from the energy integration per unit mass of fissile material. This results from the depletion/creation of fissile material which inherently occurs with time, even without neutron irradiation. In using burnup as a time step, the code-user must adjust for this behavior. In figure 2.3, the systematic errors of ^{235}U and ^{239}Pu show that a maximum burnup of 2 $\frac{MWd}{kg}$ is necessary to ensure that the time integration is small enough to resolve the change in the unit of burnup. Only minor refinement is required to capture the production of the primary fission products in a LWR case, ^{135}Xe and ^{149}Sm. Due to the often termed "cancellation of errors" [19, 23], the solution converges quite rapidly. This will be discussed in more detail with the other cases.

In figure 2.4, the total flux magnitude (a) and relative error in the reaction

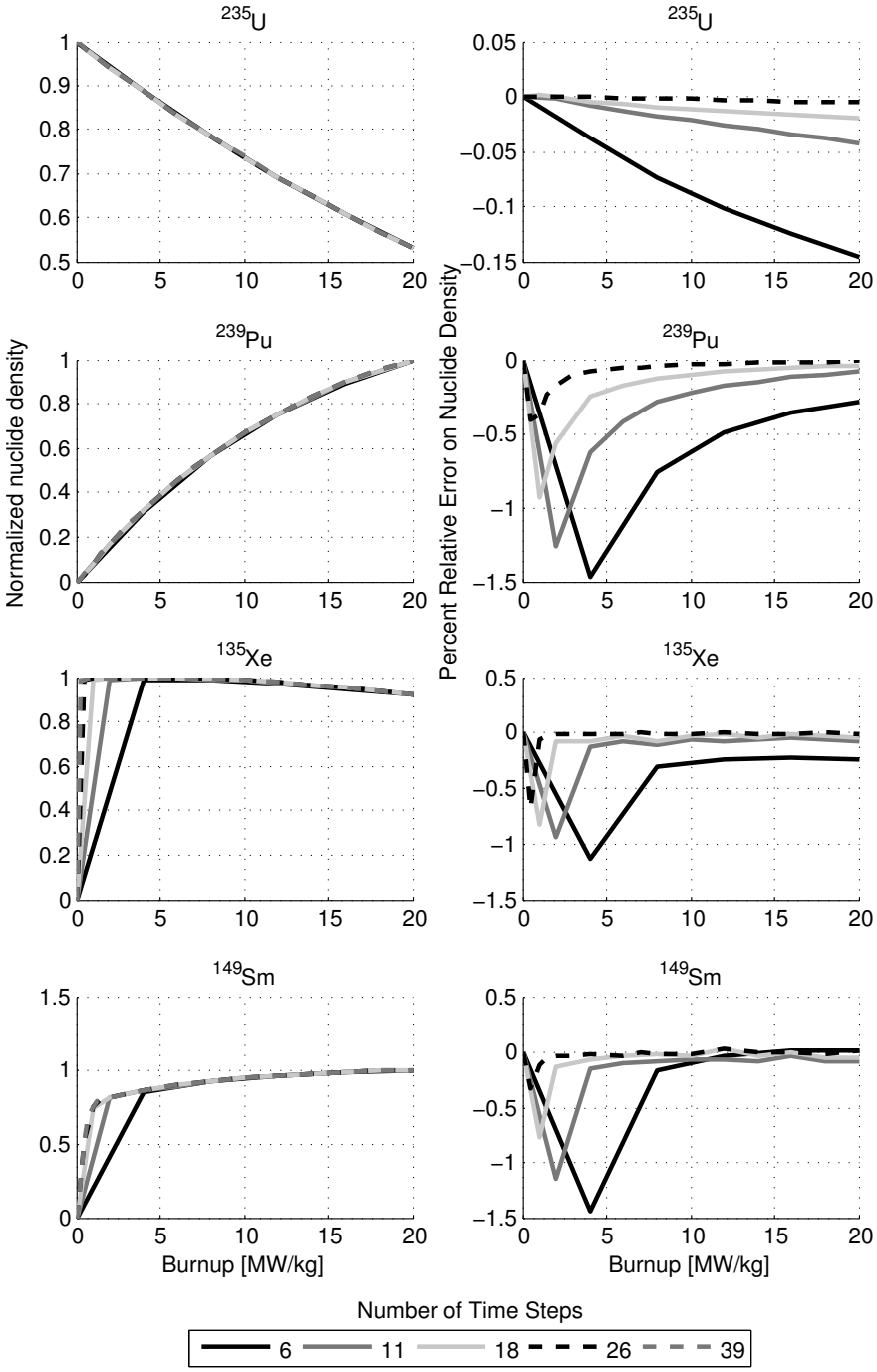

Figure 2.3: Select nuclides in SF95 of 17x17 LWR lattice without burnable absorber rods.

rate (b) for the case with 19 time steps (c) and the case with 6 time steps (d) are shown at a time step of 8 $\frac{MWd}{kg}$ over a quarter of the LWR assembly. The relative difference plot shows that the reaction rates between these two cases are dominated by statistical variations rather than temporal systematic errors. The flux and reaction rate distributions are quite uniform, owing to the reflective boundary conditions and long mean free path of the neutrons throughout the assembly.

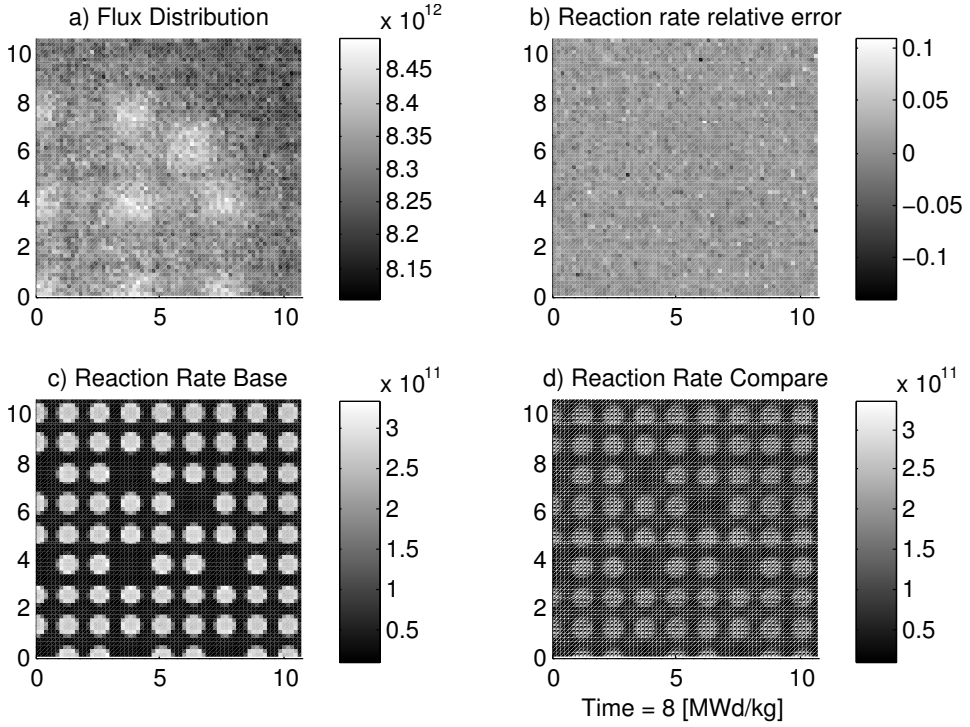

Figure 2.4: Absorption rate and flux comparison for two 17x17 LWR lattice cases without burnable absorber rods at 8 $\frac{MWd}{kg}$.

Overall, the temporal resolution of a case without burnable absorbers can be quite coarse. The neutron transport solution and the depletion solution are loosely coupled in this case. If the reactor designer needs only to worry about the EOL predictions

from an operational standpoint, very few time steps are necessary. However, in order to capture the long-term behavior of the nuclide densities, more refinement is required to reduce the systematic errors that arise from the coupling time integration scheme. This most likely arises from the use of burnup as a unit of time. Inherently, the normalization for burnup will change as the fissile inventories are depleted/created. The changes in the fissile inventory results in changes in the total energy released per fission. In order to maintain burnup as a time step, the time step must be sufficiently small that inventory changes do not affect the power integration (or change in the Q-value). Addressed here and in [19], a unit of 2 $\frac{MWd}{kg}$ provides sufficient resolution to capture the energy integration. It is, therefore, recommended that a maximum burnup time step of 2 $\frac{MWd}{kg}$ be applied to this methodology.

2.1.2 Standard 17x17 lattice with burnable absorbers

The next case includes the burnable absorber rods containing Gd_2O_3/UO_2, which is shown in figure 2.5. This case uses the dimensions and materials from the NEA benchmark and no special treatment is given to the geometry to account for self-shielding and radial/azimuthal depletion. However, compared to the previous case, the burnable absorber rods have been added to match the NEA benchmark specifications. The SF95 rod location is still used for analysis in this section.

The calculation of multiplication factor as a function of burnup are shown in figure 2.6 in a similar format presented in the previous section. It is evident that significant systematic errors arise when the Gd in the burnable absorber has depleted sufficiently to negligibly impact the neutron transport solution (9-12 $\frac{MWd}{kg}$), as shown in figure 2.7. This behavior results in a large neutron flux shift; therefore, more temporal refinement is required for the neutron transport solution to capture the change in the reaction rates, nuclide densities, and the multiplication factor.

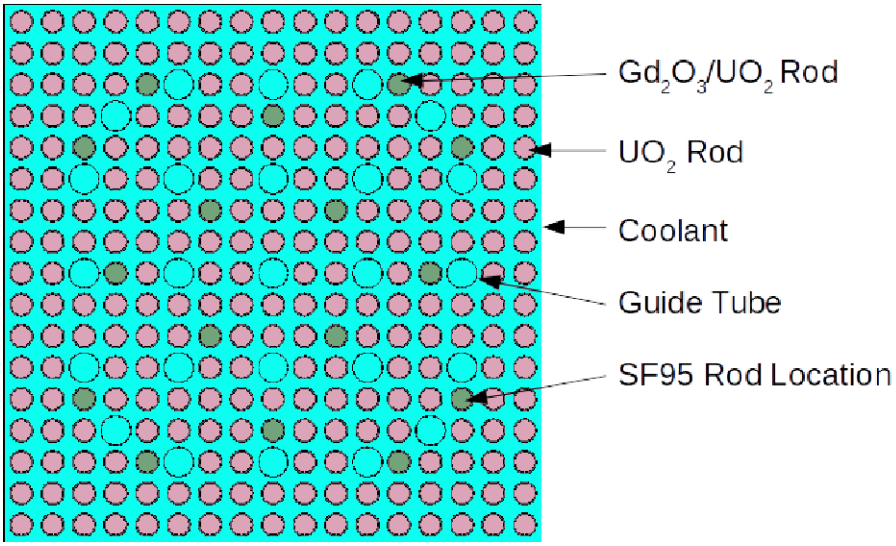

Figure 2.5: Geometry of 17x17 LWR lattice with burnable absorber rods and no spatial discretization.

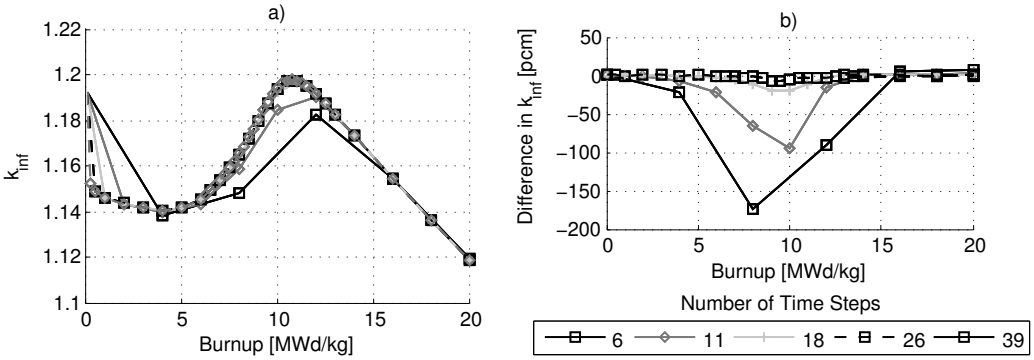

Figure 2.6: Infinite multiplication factor of 17x17 LWR lattice with burnable absorber rods and no spatial discretization.

In figure 2.7, the normalized nuclide densities for ^{155}Gd and ^{157}Gd are shown along with the relative difference compared to the high level of refinement. This shows that the time step size must be reduced in order to reduce the systematic error and converge the nuclide behavior in the burnable absorbers.

In figure 2.8, the nuclide concentration in the SF95 rod is shown for a few select

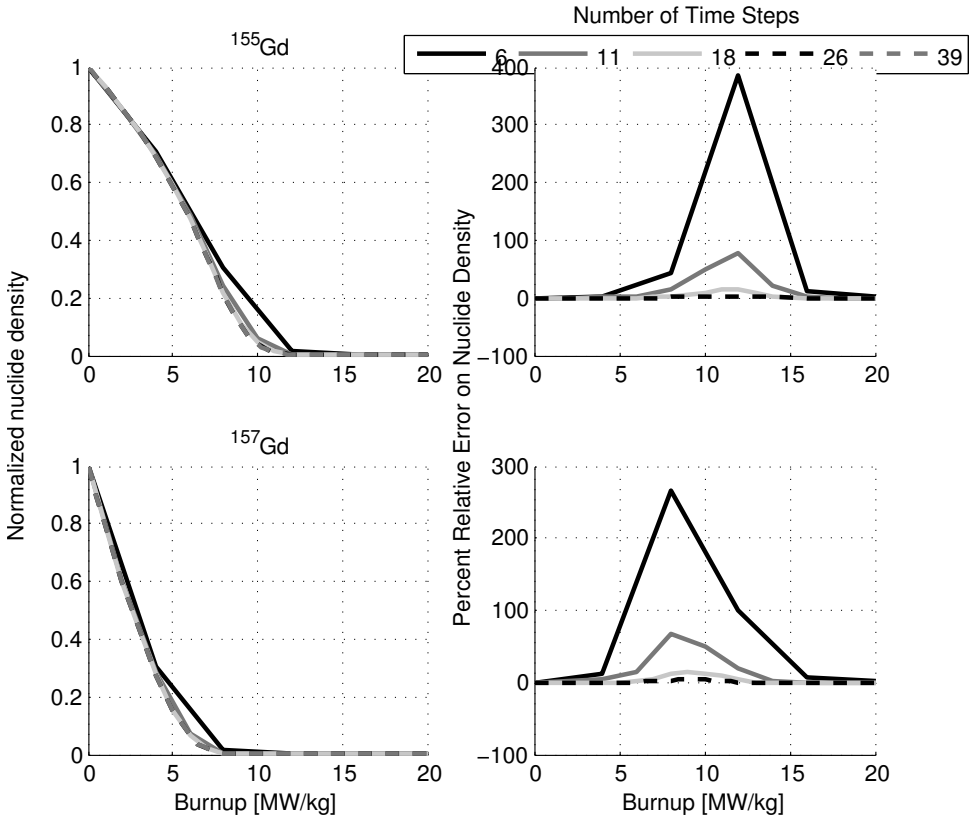

Figure 2.7: ^{155}Gd and ^{157}Gd normalized nuclide densities and relative differences in pin SF95.

nuclides with a similar format as in the previous section. It is evident that the systematic errors dominate compared to the statistical errors contrary to what was seen in section 2.1.1. This results from the tight coupling of the neutron transport solution to the depletion calculation, since the burnable absorber introduces large spatial gradients in the neutron flux as shown in figure 2.9.

In this figure, the flux depression (a) results from the addition of the burnable absorbers. The flux is shown for the most refined case with 39 time steps and the computed error (b) is relative to the coarsest case with 6 time steps. This figure shows the initial, no-burnup ($0\ \frac{MWd}{kg}$), flux and reaction rates. Therefore, the relative error plot shows the statistical error in the reaction rate as a result of the numerical

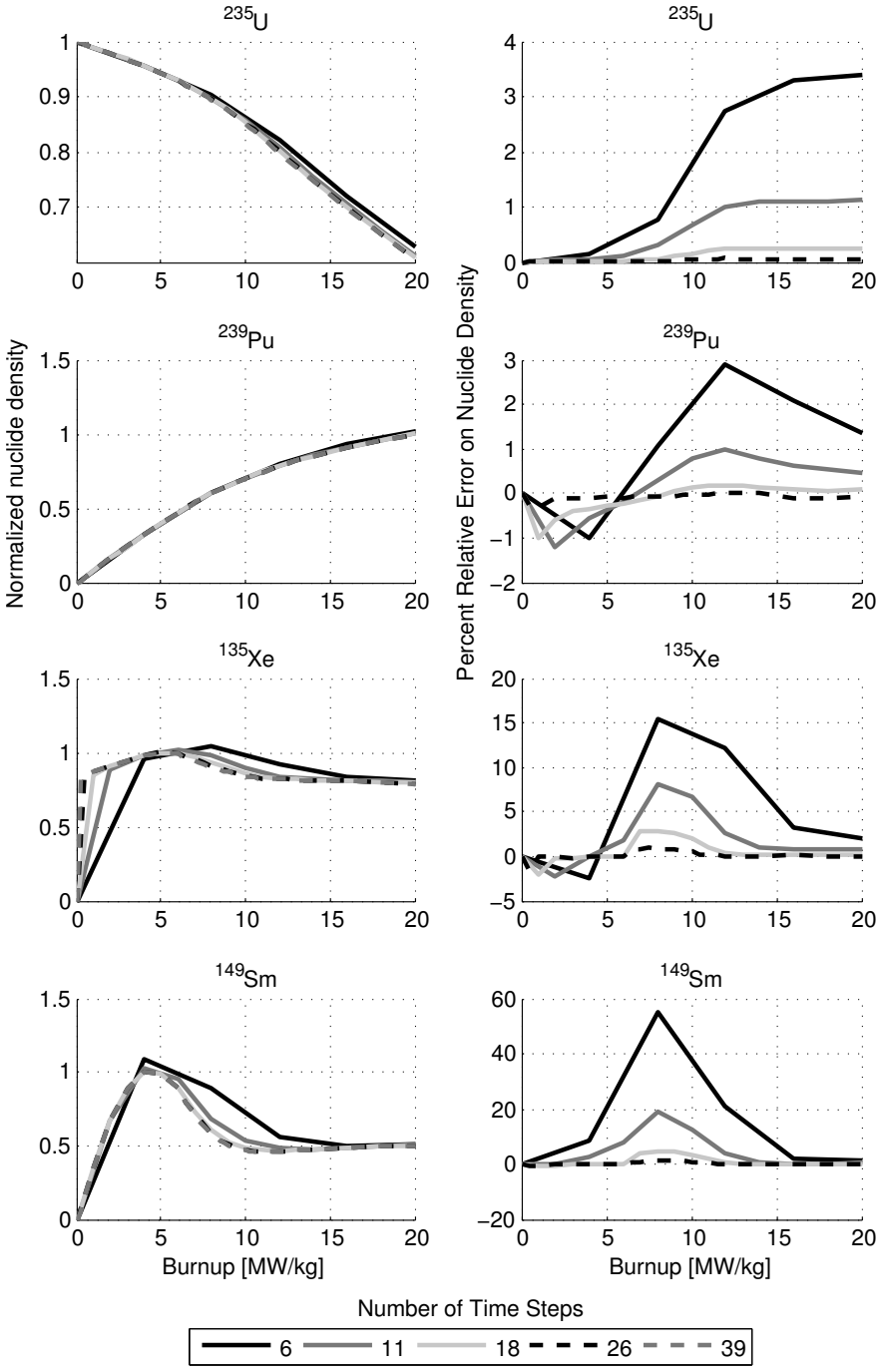

Figure 2.8: Select nuclides in SF95 of 17x17 LWR lattice with burnable absorber rods and no spatial discretization.

convergence. The reaction rate gradient in the burnable absorbers, (c) and (d), show that there is a strong spatial gradient and precludes the use of spatially discrete cells to resolve the spatial nuclide density distribution in these pins. This will be the subject of the next test case.

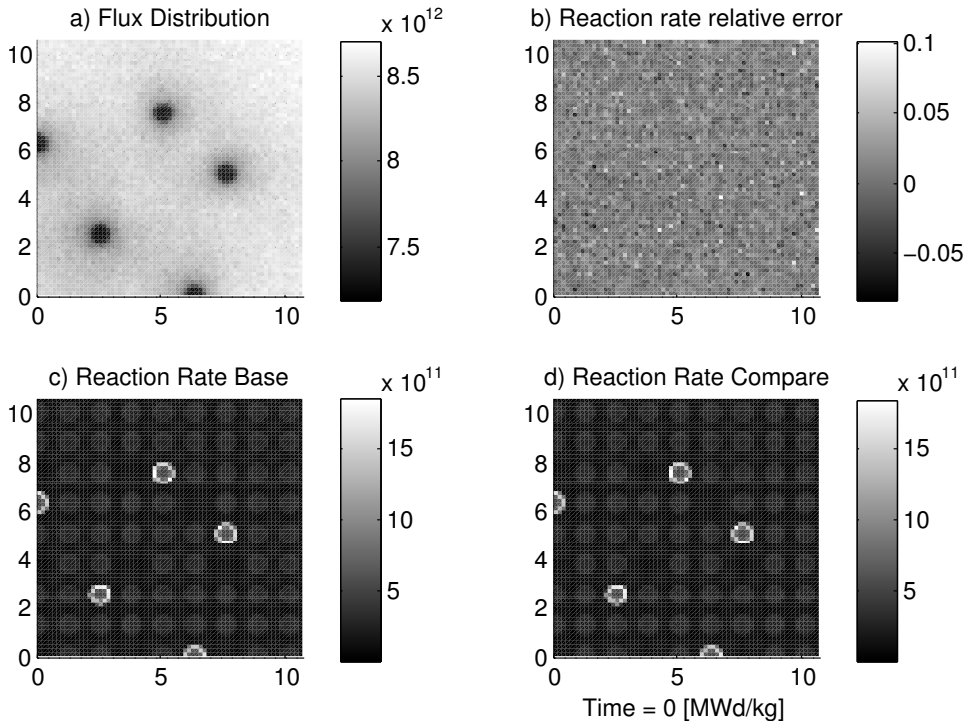

Figure 2.9: Absorption rate and flux comparison for two 17x17 LWR lattice cases with installed burnable absorbers at 0 $\frac{MWd}{kg}$.

In figure 2.10, the flux (a) and relative difference in reaction rate (b) for the case with 37 time steps (c) and the case with 6 steps (d) is shown at a time step of 12 $\frac{MWd}{kg}$ for a quarter of the assembly. This shows that in (a) the overall flux depression resulting from the absorption in the burnable absorbers (b) is very small. At a burnup of 12 $\frac{MWd}{kg}$, the Gd has been depleted to negligible levels; therefore, loosening the coupling between the neutron transport and depletion solution. For

the coarse case, however, this behavior has not yet been fully resolved, demonstrating the need for increased temporal resolution.

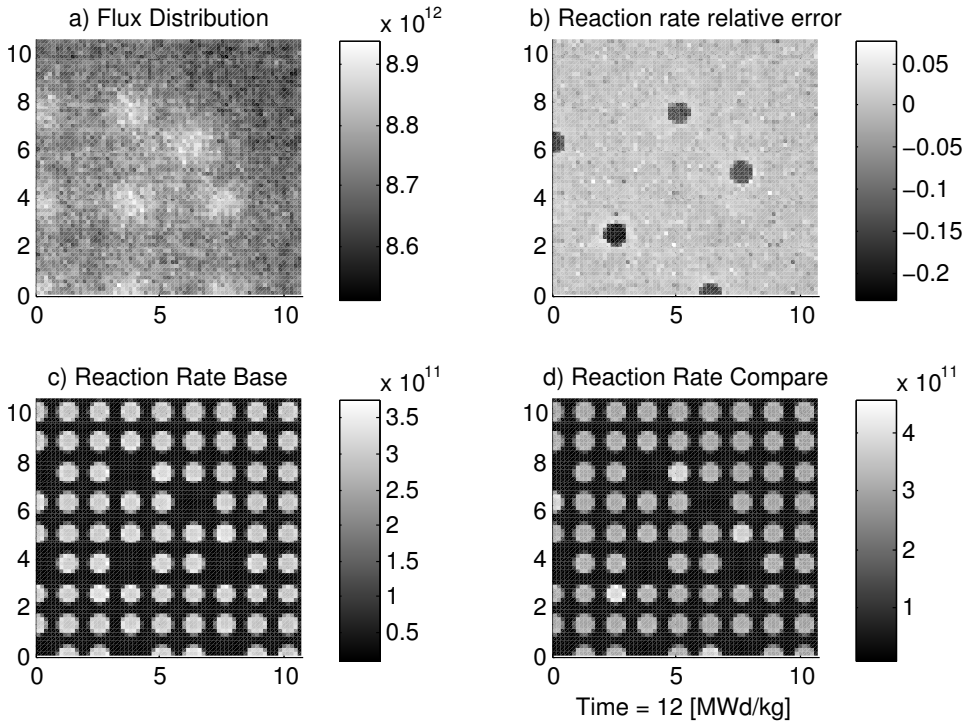

Figure 2.10: Absorption rate and flux error comparison for two 17x17 LWR lattice cases at 12 $\frac{MWd}{kg}$.

With the infinite lattice case evaluated here, in particular with the addition of burnable absorbers, the primary consideration for resolving the temporal behavior of the system is dependent on the depletion of the burnable absorbers. As demonstrated in section 2.1.1, the systematic errors from not resolving the initial fission product burn-in are small. Consequently, the resolution requirements for this case are most important for the reactor designer interested in reactor control. For example: it is necessary to ensure there is a sufficient shutdown margin at the time of peak excess reactivity or the dilution of soluble poison can compensate without introducing a

positive moderator coefficient. Without a sufficiently resolved temporal solution, the excess reactivity will be under-predicted.

2.1.3 Standard 17x17 lattice with burnable absorbers with spatial discretization

The addition of spatial discretization in the burnable absorber rods of the analysis performed in section 2.1.2 is to illustrate the impact of not resolving self-shielding. A total of 5 concentric cylinder are used with a constant volume in order to represent each spatial layer, see figure 2.11.

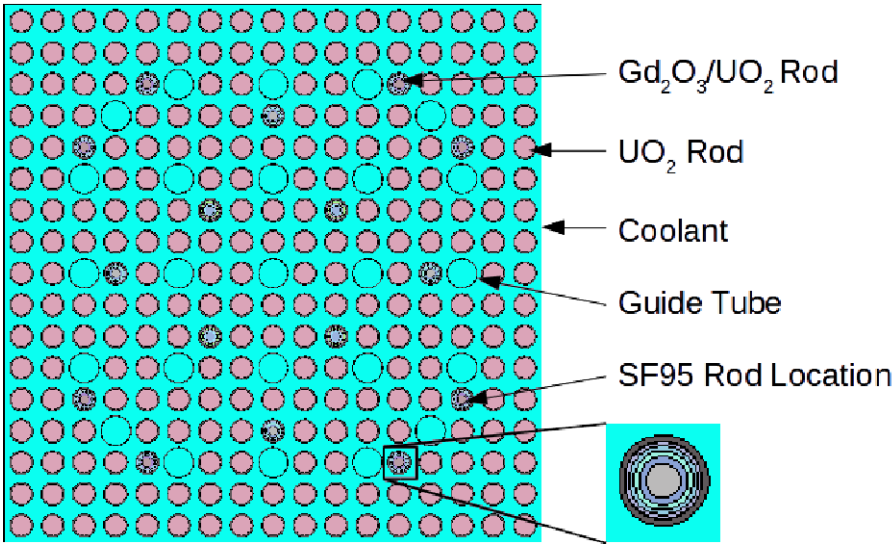

Figure 2.11: Geometry of 17x17 LWR lattice with burnable absorber rods.

In figure 2.12, the calculation of the multiplication factor is shown for each refinement level (a) along with the relative error in pcm (b). As expected, a high level of resolution is still required in order to capture the depletion of the burnable absorber. Also, the addition of spatial depletion zones used for capturing self-shielding in the burnable absorber requires even more temporal resolution. This is expected

due to the tight coupling between the neutron transport solution and the depletion calculation.

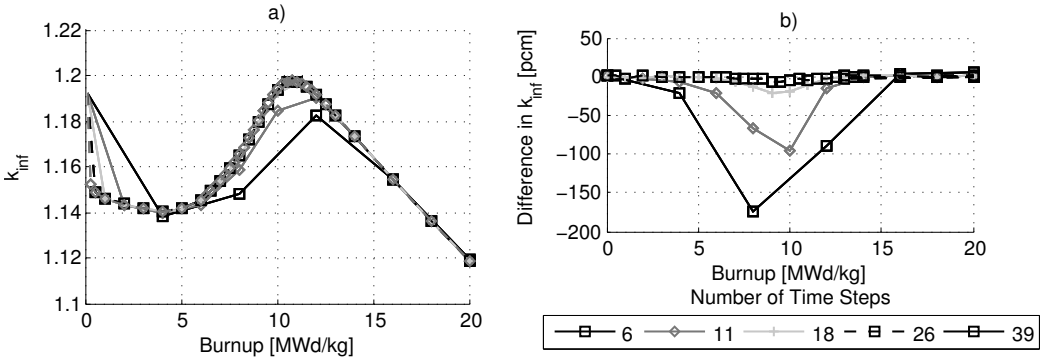

Figure 2.12: Infinite multiplication factor of 17x17 LWR lattice.

Unlike in section 2.1.2, where the Gd was depleted uniformly within the fuel pin, now there is a spatial transition from one zone to another. In other words, an outer layer is shielding the inner layers from being depleted. This transitions into a lower overall depletion rate of the burnable absorber as can be see when comparing figures 2.6 and 2.12. The approach to the maximum excess reactivity is delayed in the case with spatial discretization, since the self-shielding is being accounted for in the simulation. Moreover, when accounting for self-shielding, the systematic error is much larger, suggesting that temporal and spatial convergence studies are necessary.

Much can be said about the comparison or overall system nuclide behavior to each individual, spatial layer of the discretized burnable absorber rod; however, it is illustrative enough to look at just the inner most layer, see figure 2.13, compared to figure 2.8. The behavior is much the same, except the change in the gradient of ^{235}U is offset, resulting from the depletion of shielding layers.

The typical flux and reaction rate plots are shown in figure 2.14 comparing the

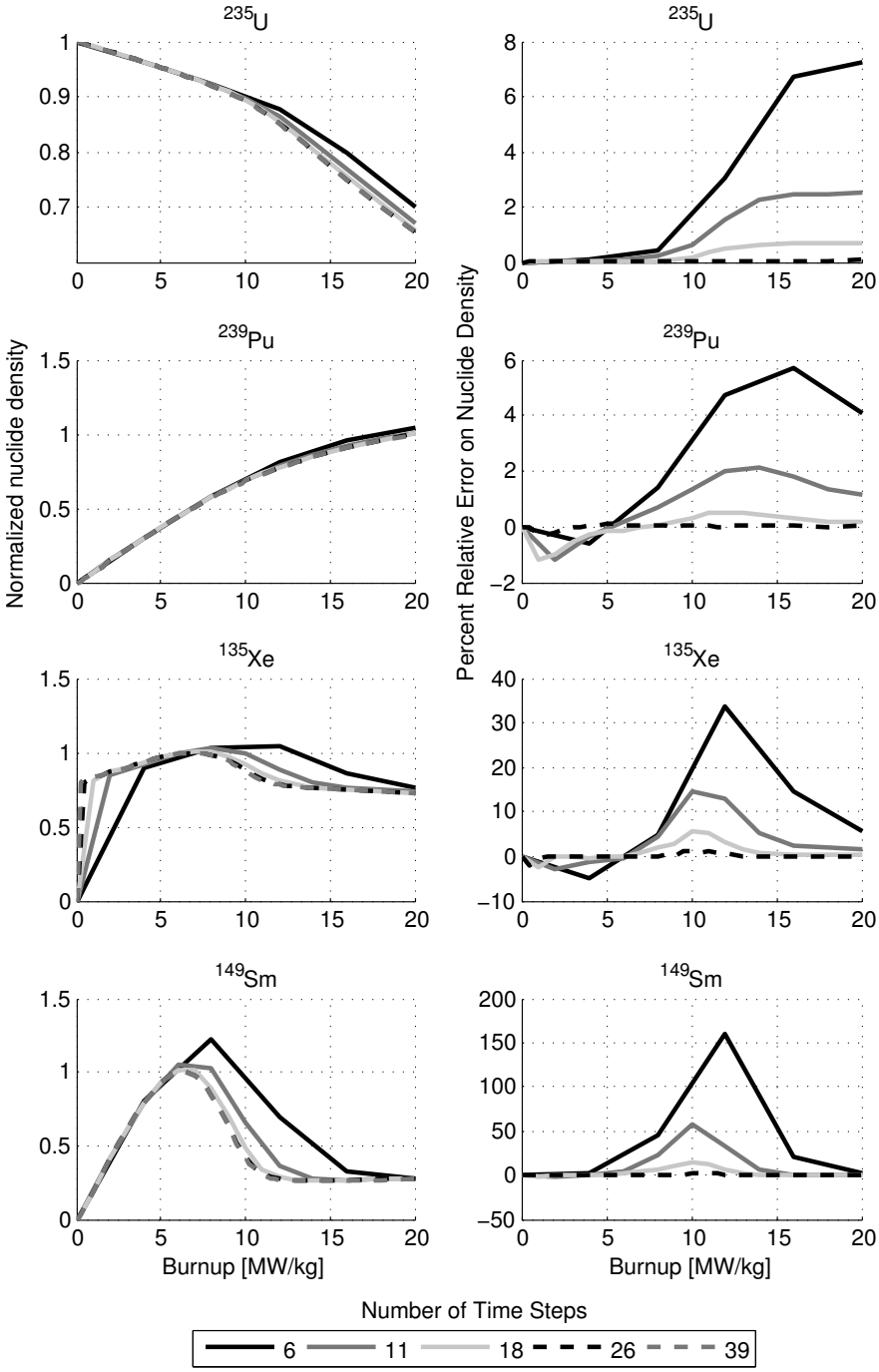

Figure 2.13: Select nuclides in the central spatial layer of SF95 of 17x17 LWR lattice.

coarsest temporal resolution to the finest at a burnup of 12 $\frac{MWd}{kg}$, where the concentration of Gd for all but the inner most layer has a negligible impact on the neutron transport solution. The magnitude of the error in the reaction rates is very high compared to previously studied cases.

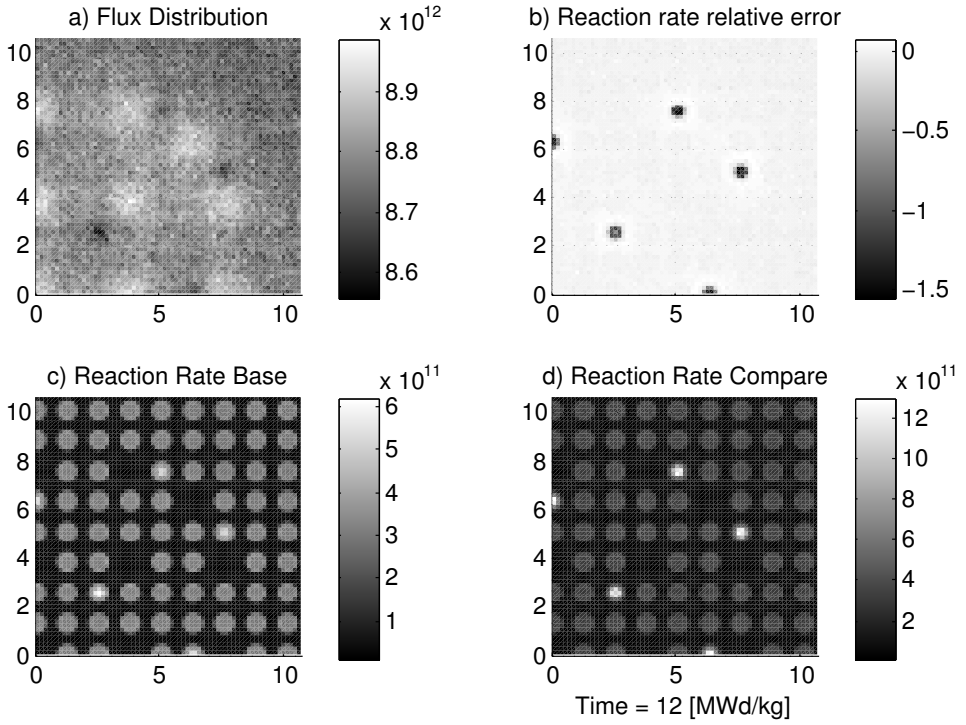

Figure 2.14: Absorption rate and flux error comparison for two 17x17 LWR lattice cases at 12 $\frac{MWd}{kg}$.

In the 17x17 lattice case with spatially discretized burnable absorbers to account for self-shielding, the time step requirements are increased compared to the previous case without spatial discretization. As expected, the time step requirements are still dominated by the depletion of the burnable absorber, resulting from the tight coupling in the neutron transport and depletion calculations. Also, there are added

spatial effects in the burnable absorber that are not present in the previous simulations. This additional behavior has to be resolved in the temporal space and the added degree of freedom in the spatial distribution of the nuclide density increases the need for more time steps.

2.1.4 Reduced 3x3 lattice with burnable absorbers and spatial discretization

The final case to be assessed is a small 3x3 lattice with the same dimensions and materials for each pin as the NEA benchmark, shown in figure 2.15. However, one of the nine pins is a burnable absorber rod and is spatially discretized to account for self-shielding. As performed in the previous simulations, the fuel pins are not spatially discretized. The importance of this model is to test the developed methodology for a case in which the behavior of the system is completely dependent on a very high reaction rate component. This forces the depletion and neutron transport solutions to be very tightly coupled. In addition, the boundary conditions for this case are reflected boundary conditions. This forces the burnable rods to be clustered and result in even steeper gradients in the thermal flux. Periodic conditions would exhibit different behavior.

In figure 2.16, the calculation of the multiplication factor is shown for each refinement level (a) along with the relative error in pcm (b). Again, the addition of strong coupling between the neutron transport solution and the depletion solution ameliorates a need for greater temporal resolution during the depletion coupled simulation. Even though this simulation is comparatively smaller in size, the required number of time steps to reach a converged solution is greater than all of the previously assessed cases. This actually fits with intuition, since the depletion and neutron transport solution are more tightly coupled in this case.

The nuclide behavior with burnup for the outer most layer of the burnable ab-

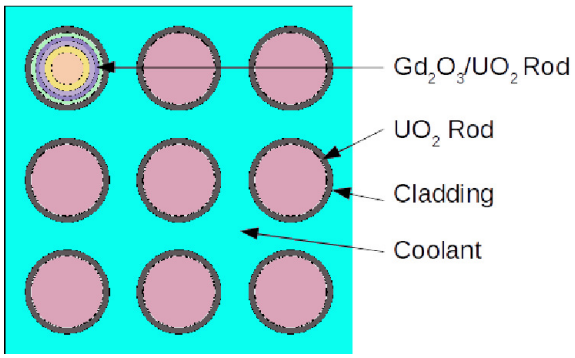

Figure 2.15: Geometry of 3x3 LWR lattice.

sorber is shown in figure 2.17. There are significant systematic errors associated with the time step resolution, resulting from the tight coupling. Since reflected boundary conditions are used, the flux depression, resulting from the burnable absorber, is very significant. In is important to note that the systematic errors in the Xe concentration are likely not a result early refinement of time steps, but rather it is a result from the systematic errors in the ^{235}U and ^{239}Pu concentrations. The fission yields for ^{135}Xe and ^{135}I differ for these two fissile materials and the resulting equilibrium is affected by their production rather than initial time step resolution.

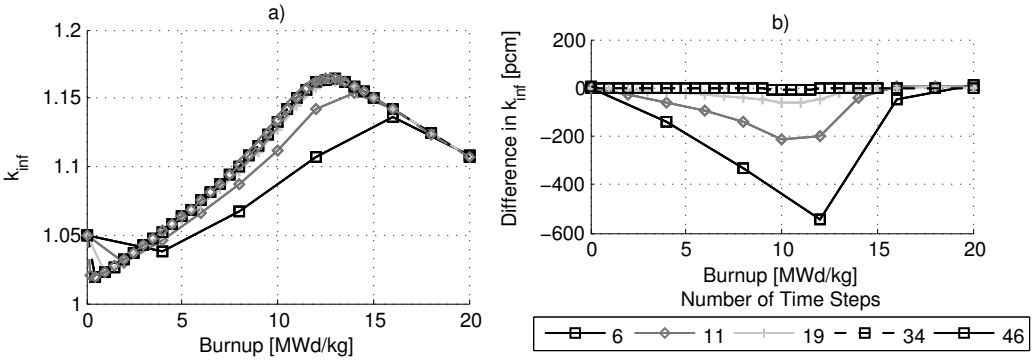

Figure 2.16: Infinite multiplication factor of 3x3 LWR lattice case.

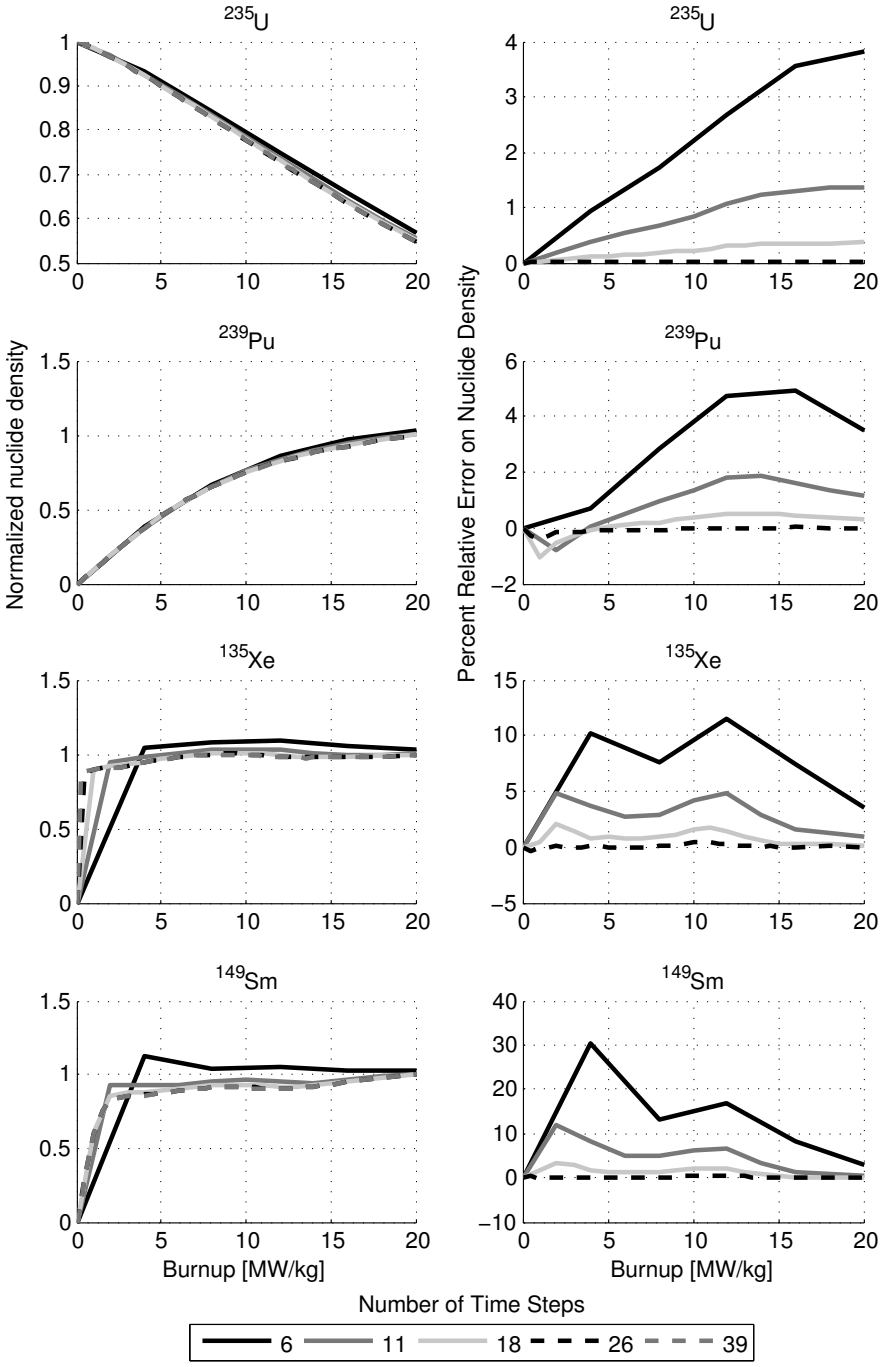

Figure 2.17: Select nuclides in outer layer of burnable absorber rod in 3x3 LWR lattice.

The tight coupling in the depletion simulation requires further refinement, particularly, when the burnup is less than a few $\frac{MWd}{kg}$. This results from the fission products taking longer to reach equilibrium in the outer layer of the burnable absorber. Equilibrium is reached when the flux shape, dependent on the nuclide distribution and concentration, reaches a nominally unvarying shape. The nuclide concentration is dependent on both the individual nuclide decay constants and the reaction rates resulting from the flux. In the case with spatial discretization, the spatial flux distribution has an additional degree of freedom. This increases the temporal refinement necessary to capture the temporally varying nuclide and flux distributions. In particular, the neutron transport solution is dominated by the depletion of the burnable rod in this small system.

2.1.5 Concluding Remarks

The conclusions from this study are enumerated here. This analysis has demonstrated that there are significant systematic errors introduced by poorly temporally refined coupled simulations. This is not a new discovery; however, it is often overlooked in many depletion calculations in favor of the much smaller statistical errors introduced by the stochastic Monte Carlo simulation method. It is demonstrated that the convergence requirements depend heavily on the system, which in itself determines the coupling between the neutron transport and depletion calculations.

It is demonstrated, though not explicitly discussed, that the requirement for highly resolved solutions is only required for detailed simulations. It turns out, for pre-conceptual analysis, coarse time steps can be quite insightful for determining some important bulk parameters. For example, if the nuclear engineer is only interested in the lifetime of the core, very coarse time steps can be used. However, these coarse simulations should not be used if the power profile is of interest. In

the previous discussions, it is shown that such coarse steps can lead to significant variations in the reaction rate density. This is detailed further in the works of Dufek [10, 12], Isotalo [19, 20], and Kotlyar [23] .

It was shown that the tightness of coupling also depends on the number of degrees of freedom in the system. It is expected that as the system gets larger, extends to 3D, or is spatially discretized, the need for further temporal resolution will be necessary in order to resolve the coupled physics behavior.

The solutions for the multiplication factor are repeated for all of the depletion cases and shown in figure 2.18. While this is not a full description of the depletion calculation, it is instructive for understanding the behavioral differences between each simulation.

The legend description is as follows:

- largeLattice: Standard 17x17 lattice with spatially discretized burnable absorbers
- smallLattice: Reduced 3x3 lattice with spatially discretized burnable absorbers
- nozones: Standard 17x17 lattice with burnable absorbers
- noBAs: Standard 17x17 lattice without burnable absorbers

The behavior resulting from the addition of burnable absorbers is clearly visible. The addition of absorbers reduces the total excess reactivity at the BOL loading, allowing for more fissile material without having to include more control material. The burnup of the BAs occurs, in this case, over a burnup of approximately 12 MWd/kg. During this time, the spatial flux distribution is impacted by the high reaction rate within the burnable absorber rods. The result is a tightly coupled depletion and neutron transport response. This requires more time steps. In effect,

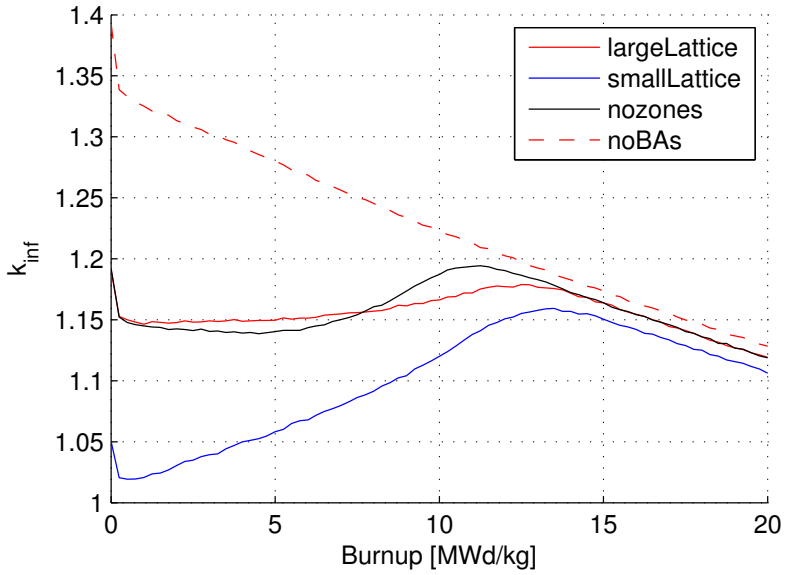

Figure 2.18: Infinite multiplication factor for all tested cases as a function of burnup.

the smallLattice required the highest number of time steps, despite being a much smaller problem geometrically. This is because the single burnable rod impacts the flux distribution over the entire modeled system. The time step sizes are shown in figure 2.19 for each of the fully resolved cases.

The length of the time step is limited to the integration of the energy released during the time interval. Inherently, burnup is a unit dependent on the energy integration, which changes as a function of the fissile material in the fuel. As a result of neutron irradiation, the average Q-value, the energy released from fission, changes with the fissile constituents. In particular, neutron capture with fertile ^{238}U results in the production of fissile ^{239}Pu. Later in the fuel life, a significant portion of heat is generated from the Pu. The time step must be limited in size such that the error introduced from the energy integration remains small. This is system dependent and for the LWR case analyzed here should be limited to 2 MWd/kg. In systems

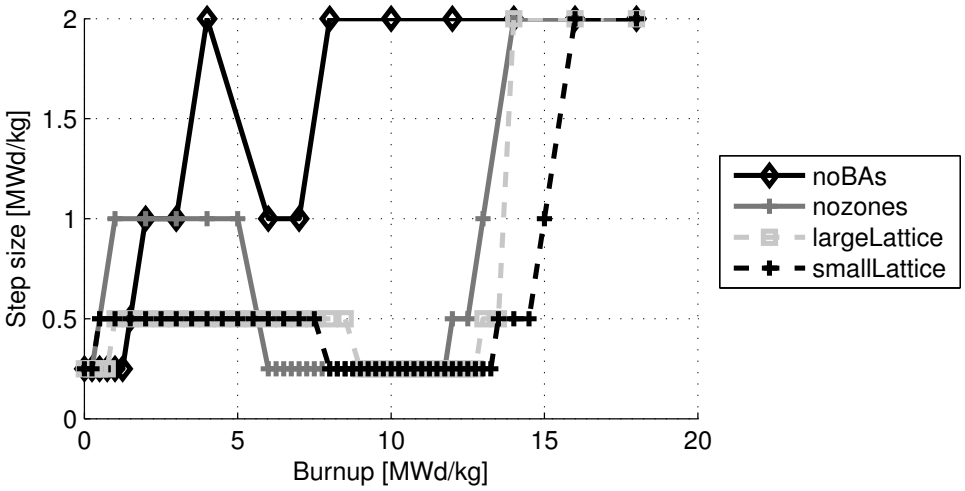

Figure 2.19: Time step size as a function of burnup for more refined cases.

with more significant breeding and conversion capabilities, this limit may need to be adjusted.

There are some other concerns that have not been addressed. Namely, there is a time constant associated with the approach to equilibrium of some major fission products, particularly ^{149}Sm. The lag time in Sm is very noticeable in many of the above calculations. This can inevitably impact the time-step selection for systems that vary in reactor power. Another issue that is not addressed is simply the application to other reactor systems. In general, fast reactor systems do not require as small time steps due to the rather long mean-free path length of the neutrons. This largely decouples the neutron transport and depletion calculations. On the contrary, systems like the heavy-water reactor and graphite moderated reactor, the neutron transport and depletion calculations tend to be more tightly coupled resulting from higher thermal fluxes, despite typically having longer mean free path lengths than in a conventional LWR system.

2.2 Methodology

For the remainder of this section, these four cases will be considered collectively to ensure each case can be handled by the algorithm. The methodology modifies the mid-point predictor-corrector with an additional parameter evaluation which will predict a new time step. For this reason, another burnup calculation is required to update the depletion sequence. The method can be implemented into the mid-point method, in the following manner:

for $i := 0$ to $MaxStep$ do

$initialStepsize = h$

solveNeutronTransport(N_{BOS}) output: $\phi^P(\mathbf{r}, t_i)$

solveMatrixDepletion$(\phi^P(\mathbf{r}, t_i), N_{BOS})$ output: $N^P(\mathbf{r}, t_i + h)$

updateTimeStep() output: $t_{i+1} = t_i + h'$

solveMatrixDepletion$(\phi^P(\mathbf{r}, t_i), N_{BOS})$ output: $N^P(\mathbf{r}, t_i + h')$

solveNeutronTransport$(N^P(\mathbf{r}, t_i + h'))$ output: $\phi^C(\mathbf{r}, t_{i+1})$

interpolateFlux$(\phi^P(\mathbf{r}, t_i), \phi^C(\mathbf{r}, t_{i+1}))$ output: $\phi(\mathbf{r}, t_{i+1/2})$

solveMatrixDepletion$(\phi(\mathbf{r}, t_{i+1/2}), N_{BOS})$ output: $N(\mathbf{r}, t_{i+1})$

end

For this methodology to be as efficient as possible, the new time step should be computed after the first depletion calculation:

$$t_{i+1} = t_i + h' = t_i + h \times p \tag{2.1}$$

where p is the correction parameter used to adjust the time step in the function updateTimeStep(). A flow chart shows this method again in figure 2.20, which is repeated for each burnup time step.

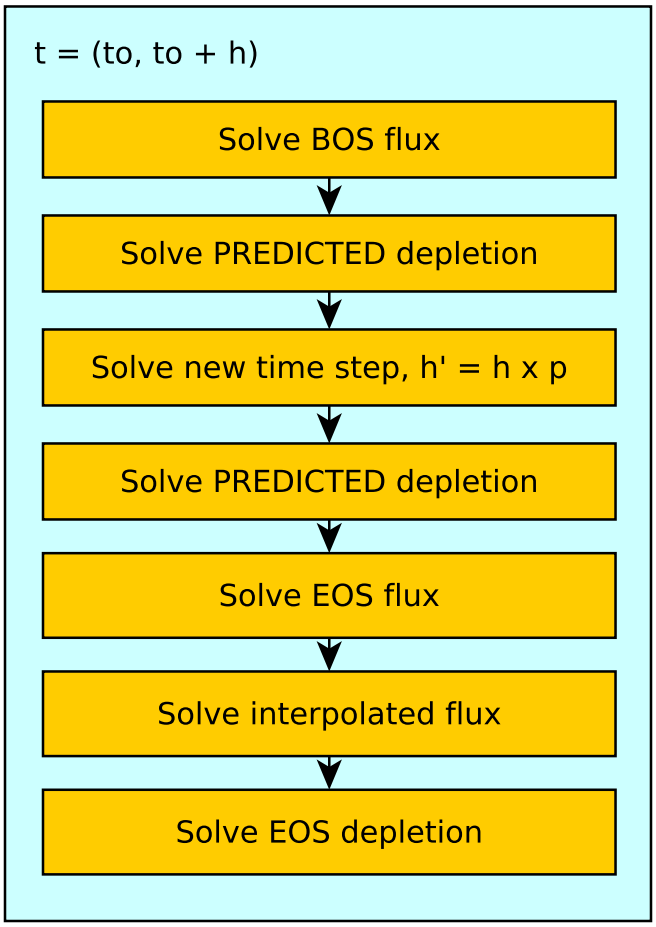

Figure 2.20: Time step size as a function of burnup for more refined cases.

The first depletion calculation is required to determine various reaction rate gradients and spatial effects resulting from the predicted neutron flux distribution. These parameters are evaluated and the result is a time step used to adjust the calculation of the predicted nuclide densities to ensure a close-to-temporally converged solution.

The second depletion calculation is then required to update the nuclide densities with the new burnup time step so that the corrector-step neutron transport can be performed on the new, predicted time step.

2.3 Development of Time Step Parameterization

The typical behavior of a thermal-neutron depletion simulation with burnable absorbers is shown in figure 2.21. There are effectively five regions of interest for developing a predictive method. These regions are determined based on the primary physical effects that dominate the eigenvalue behavior: 1) burn-in of fission products, 2) transition from fission-products to burnable absorbers, 3) burnable absorbers, 4) transition of burnable absorbers to fissile depletion, and 5) fissile depletion.

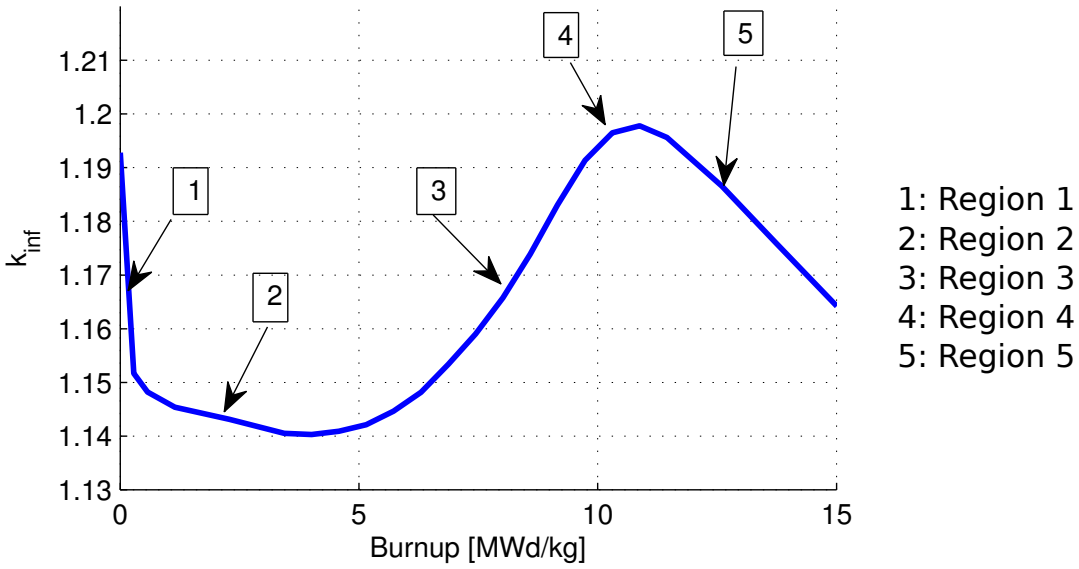

Figure 2.21: Depletion curve for a PWR 17x17 infinite lattice simulation.

2.3.1 Description of Regions of Interest

When fresh fuel undergoes initial irradiation, fission products begin to contaminate the fuel (region 1). In a thermal-neutron spectrum, this can have a dramatic effect on the reactor behavior and spatial neutron flux distribution. There are two primary fission product of interest in this region: ^{135}Xe and ^{149}Sm, which will be referred to only as Xe and Sm throughout section. With a constant flux approximation, the time constants for these nuclides during irradiation can be determined:

$$\tau_{Xe} = \frac{1}{\lambda_{Xe} + \sigma_{a,Xe}\phi} \tag{2.2}$$

$$\tau_{Sm} = \frac{1}{\sigma_{a,Sm}\phi} \tag{2.3}$$

The time constant is dependent on the flux magnitude and is considerably smaller for Xe. Therefore, the initial behavior of this region is dominated by the build up of Xe. As Sm begins to reach equilibrium, the behavior begins to transition to the burnable absorber region (region 2). The behavioral response of the system in both region 1 and 2 is related to the rate of change of the absorption reaction rate which is proportional to the neutron fission rate density. This suggests that these can be represented by an integral parameter.

Regions 3 and 4 are dominated by the depletion of the burnable absorbers. These absorbers introduce large spatial gradients in the reaction rates and neutron fluxes over the system, as described in the previous section. Region 4 behavior is prescribed by the depletion of the burnable absorbers to the point that the installed poison has a negligible impact on the neutron transport solution so that the behavior transitions to region 5. Region 5 is completely dominated by fissile nuclide depletion, which

takes on a linear relationship with burnup and can be computed with rather long time steps in an infinite lattice calculation.

2.3.2 Representation of the Regions

The reaction rates over the system and for each cell will be specified as:

$$R_f(t) = \int_{R^3} \int_0^\infty \Sigma_f(\mathbf{r}, E, t)\phi(\mathbf{r}, \mathbf{E})dEdV \tag{2.4}$$

$$R_a(t) = \int_{R^3} \int_0^\infty \Sigma_a(\mathbf{r}, E, t)\phi(\mathbf{r}, \mathbf{E})dEdV \tag{2.5}$$

$$R_{a,k}(t) = \int_{R_k^3} \int_0^\infty \Sigma_{a,k}(\mathbf{r}, E, t)\phi(\mathbf{r}, \mathbf{E})dEdV \tag{2.6}$$

where k is the cell. In the rest of this section, there is no distinction between the predictor and the corrector step in the integration method. The reason for this is that this method lives completely in the predictor step, using constant-in-time, predicted scalar flux, $\phi = \phi(t_o)$. The beginning of step is represented by t_o and the end of step as $t_1 = t_o + h$, where h is the step size. In an effort to save memory and computational effort, only the tracked, burnable materials are included when determining the reaction rates, such that:

$$R_a(t) = \sum_{k=1}^{M} R_{a,k}(t) \tag{2.7}$$

where M is the number of burnable zones.

The system-wide "pseudo" multiplication factor for the burnable materials can be found during the beginning of step:

$$k_p(t_o) = \frac{R_f(t_o)}{R_a(t_o)} \tag{2.8}$$

which is shown, normalized to $k_p(0)$, for the cases of interest in figure 2.22. There is a notable trend with dependence of the multiplication factor shape with the time-resolution. For example, the noBAs case requires the least number of time steps and it has a continuous downward behavior. Conversely, the smallLattice case required the greatest number of time steps.

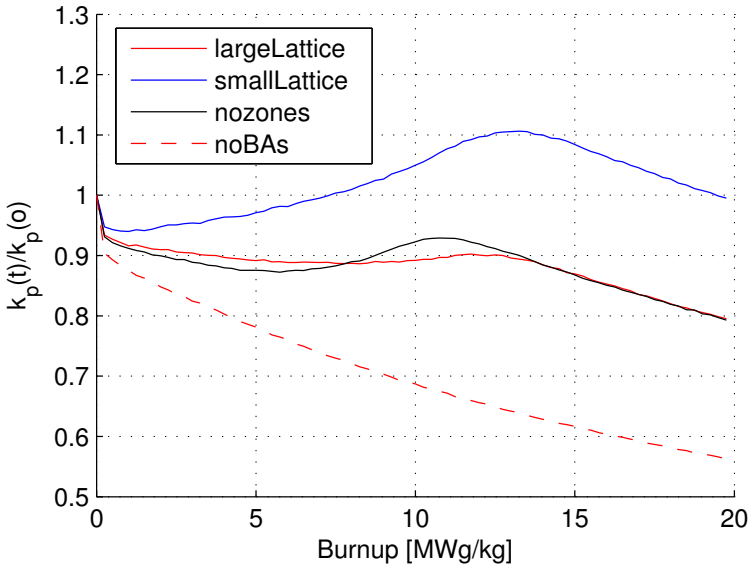

Figure 2.22: Pseudo multiplication factor as a function of burnup.

The difference in the pseudo multiplication factor between the BOS and EOS calculations can be found:

$$dk_p(t_1) = \frac{R_f(t_1)}{R_a(t_1)} - k_p(t_o) \tag{2.9}$$

This result is plotted in figure 2.23, with any evaluation less than zero set equal to zero. The importance of this parameter is to determine the gradient in the pseudo multiplication factor with time, providing insight of the strength of coupling between

the neutron transport and depletion simulations. In addition, this function provides insight of when the solutions begins to become fissile depletion dominated.

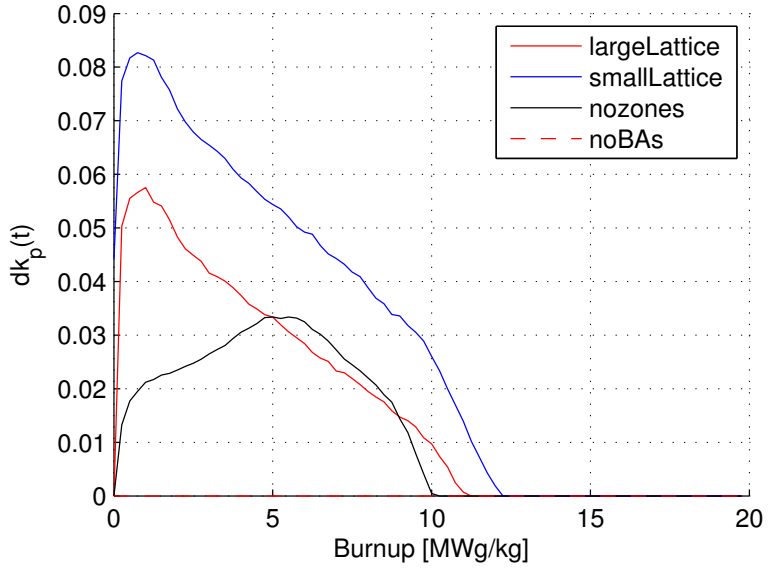

Figure 2.23: Pseudo multiplication factor difference between BOS and EOS as a function of burnup.

This parameter becomes the first component of the time step size selection function:

$$p_1 = \begin{cases} C_1 dk_p(t) & \text{for } dk_p(t) \geq 0, \quad (2.10) \\ 0 & \text{for } dk_p(t) < 0. \quad (2.11) \end{cases}$$

where C_1 is a fitting parameter.

In order to capture the spatial effect from the burnable absorbers, a peaking factor for the absorption reaction rate is introduced:

$$\hat{R}_a(t_o) = max(R_{a,k}(t_o)) \tag{2.12}$$

$$\bar{R}_a(t_o) = \frac{R_a(t_o)}{M} \tag{2.13}$$

$$fR_a(t_o) = \frac{\hat{R}_a(t_o)}{\bar{R}_a t_o} \tag{2.14}$$

The $fR_a(t_o)$ is plotted normalized to $fR_a(0)$ in figure 2.24. As expected, the noBAs case exhibits little change with burnup, since it does not have any installed burnable absorbers. There are bumps in the curves of largeLattice and smallLattice which arise as a result of the self-shielding phenomena. Since each layer is discrete in its representation, the depletion of subsequent layers can be seen.

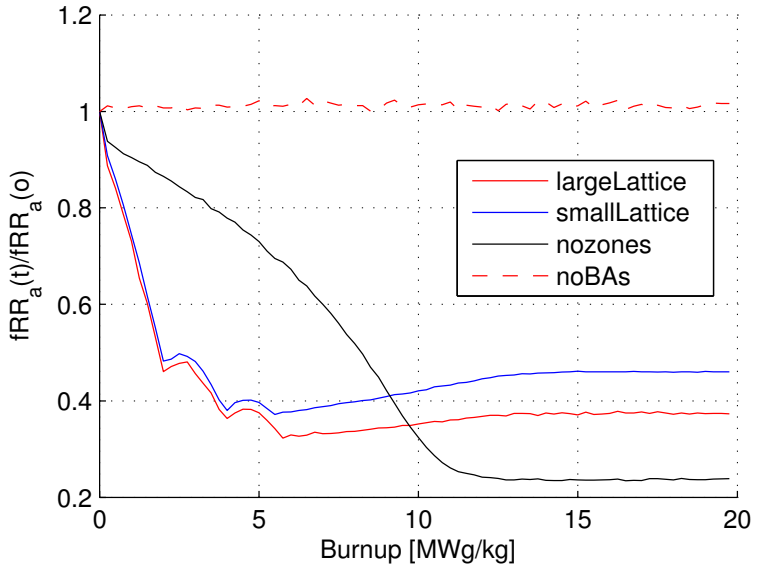

Figure 2.24: Absorption peaking factor as a function of burnup.

Another parameter is introduced, which provides a weighting based on the change

of the absorption reaction rate between the BOS and EOS calculations:

$$f_a(t_1) = \frac{R_a(t_1)}{R_a(t_o)} \tag{2.15}$$

This parameter, so far unlike the parameters shown above, requires the depletion solution, found at $t_1 = t_o + h$, where the time step, h, might be $2\frac{MWd}{kg}$, the maximum suggested depletion step. This parameter is shown normalized to $f_a(0)$ in figure 2.25.

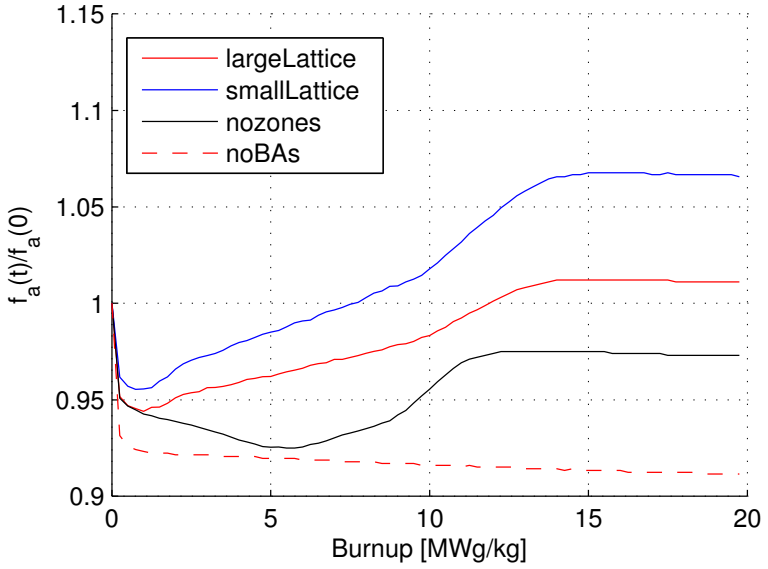

Figure 2.25: Absorption depletion weighting factor as function of burnup.

With these parameters, the second component of p can be determined:

$$p_2 = C_2 \left(\frac{fR_a(t_o)}{fR_a(0)}\right)^{C_3} \left(\frac{f_a(t_1)}{f_a(0)}\right)^{C_4} \left(\frac{k_p(t_o)}{k_p(0)}\right) \tag{2.16}$$

where C_2 and C_3 are additional fitting coefficients. This parameter attempts to describe the impact of the absorption from both installed and fission-introduced

poisons. The coefficients are used in order to impart importances on each of the terms of this parameter. The coefficient are not physical, however, care was taken to ensure the resulting parameters are dimensionless.

This function is shown in figure 2.26, using the following arbitrary coefficients:

$$C_2 = 4.0$$

$$C_3 = 5.0$$

$$C_4 = 0.1$$

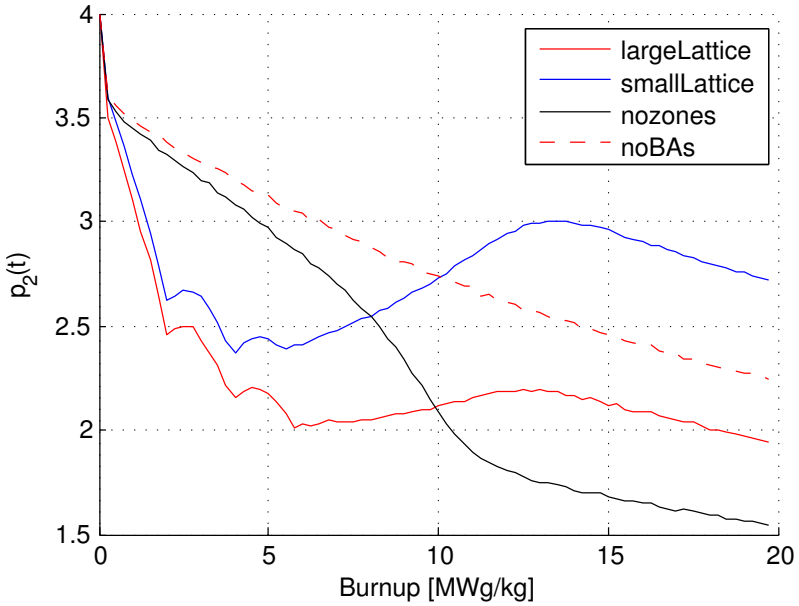

Figure 2.26: First parameter as a function of burnup.

Another parameter is formulated to determine when the depletion of the burnable absorbers occurs. This is a search parameter that tracks the relative change of the

absorption reaction rates. The search parameter is as follows:

$$sR_a(t_1) = \frac{R_a(t_1) - R_a(t_o)}{R_a(t_o)} \tag{2.17}$$

This parameter requires the prediction of the depletion just like f_a. This is plotted in figure 2.27. Note that the noBAs case does not cross the abscissa. This is an expected result, since the evaluation of the absorption reaction rate between depletion steps should typically be increasing for cases without heavy absorbers.

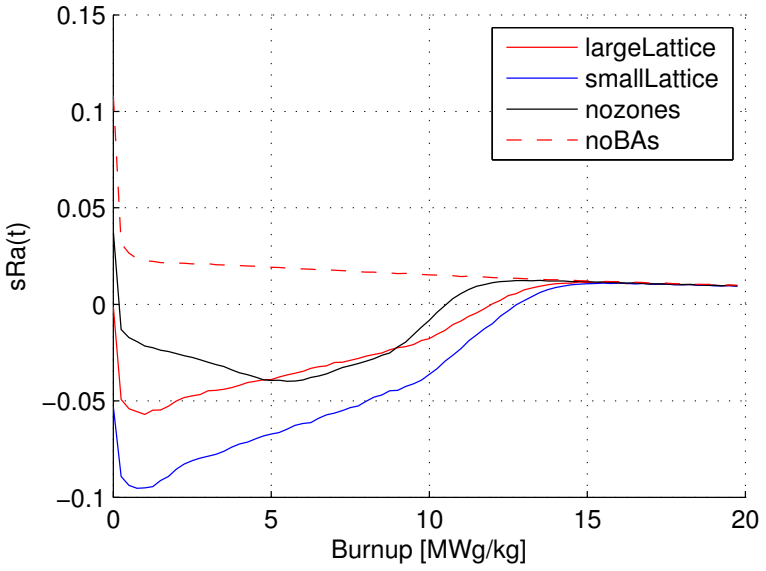

Figure 2.27: Preliminary search parameter as a function of burnup.

Comparing to results from the study in section 2.1, the behaviors for the various cases are expected. The impact of fission production production is evident and the behavior for the spatially discretized cases, accounting for self-shielding, is qualitatively acceptable. Moreover, when the fissile depletion dominated region is reached,

the solution approaches an asymptotic value. This value is likely system specific and should be addressed for other reactor system types.

The final parameter needed is used to help force the appropriate time step by determining when the system behavior is fissile depletion dominated. Its formulation is as follows:

$$p_3 = C_5 \left[1 - \left(\frac{R_a(t_1)}{R_a(0)} \frac{f_a(t_1)}{f_a(0)} \right) \right] \tag{2.18}$$

where C_5 is another fitting coefficient. This parameter is plotted in figure 2.28, with $C_5 = 18$. As shown, the transitions are not perfectly predicted by the parameter; however, the overall performance is good.

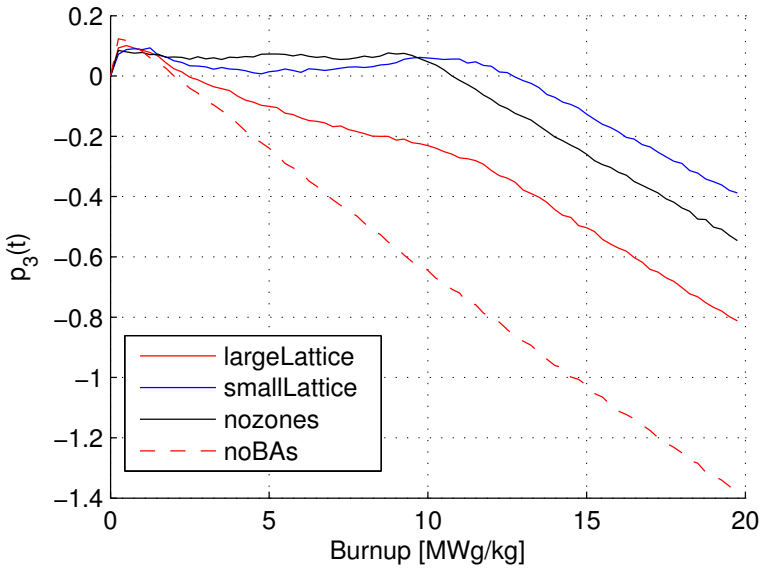

Figure 2.28: p_3 as a function of burnup.

Finally, the time stepping parameter can be determined, by manipulating equations 2.10, 2.16, and 2.18:

$$p = p_3(p_1 + 1) + p_2 \tag{2.19}$$

This parameter is plotted in figure 2.29 as a function of burnup. The constants used for this function are arbitrary and therefore the results have no physical significance in this figure.

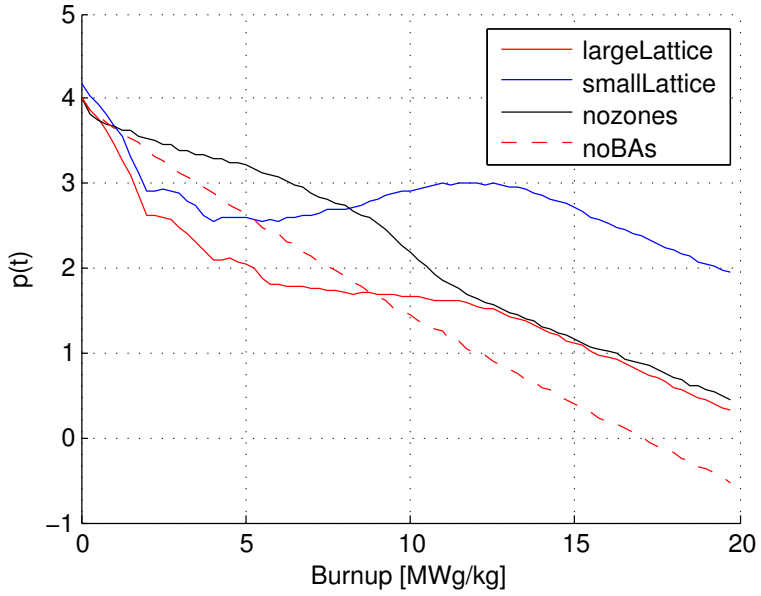

Figure 2.29: Time step correction parameter, p, as a function of burnup.

This parameter is used to correct the time step in updateTimeStep() using Equation 2.1:

$$h' = h \times p \tag{2.20}$$

This function is only the basis for determining the next time step. In the next section, the application of this function will be addressed.

2.3.3 Concluding Remarks

The new time step depends on the evaluation of the reaction rates. This inherent characteristic means that the time step prediction is subjected to the statistical errors in the neutron transport solution. As shown in analysis in section 2.1, these errors are usually quite small compared to the systematic errors associated with the temporal refinement scheme. Regardless, these statistical variations mean that with a random seed, no two simulations will have the same time steps. This makes direct comparisons between models more difficult as interpolation between time steps will be required to assess the error in any given simulation.

Overall, however, this is a rather simple formulation and can be applied to allow neutron transport and depletion coupled codes. It is not exclusive to the Monte Carlo simulation methods; however, they do stand to gain the most. In general, deterministic methods use implicit time integration which solve a non-linear set of equations and can be unconditionally stable. However, the neutron transport simulation can be costly, and this method can be applied to reduce the number of non-linear iterations that would otherwise occur.

The method still has some difficulties in region 5. The new time steps are typically smaller than necessary. This creates an unnecessary computational burden. In future developments of this method, an additional "if" statement can be used to transition to another model for calculating the predicted time step size.

3. CONCLUSIONS

The previous section demonstrated that the temporal refinement of a neutron transport and depletion coupled simulation is necessary for resolving the time-dependent behavior of both coupled physics. The tightness of coupling, or rather the need for further temporal refinement, is dependent on the system geometry, materials, and to the numerical methods used. In this dissertation, the developed method uses an infinite lattice calculation to isolate the primary materials degrees of freedom. This is performed by assessing four different light-water reactor cases. The noBAs case, without installed burnable poisons, required the fewest number of time steps for temporally converged solution. On the other hand, the smallLattice case, which was defined to demonstrate burnable absorber dominated behavior, required the most number of time steps. This directly relates the "strength" of coupled dependence between the nuclide distributions and the neutron flux distributions within the system.

A series of parameters have been developed in the previous section to attempt to capture this behavior. The methodology is implemented in this section using the Serpent 2 Monte Carlo reactor physics code. The method is tested with each of the previous four cases. These tests address the capabilities of the method to select the appropriate time step size in order to ensure a solution that is closest to being temporally converged.

The only input from the user to run a calculation with this method is the total burnup of the entire system. In addition, the user must provide what ever else is necessary for the typical geometry and material preparation. Current capabilities of this method do not allow users to accommodate other predictor-corrector numerical schemes than the mid-point formulation.

3.1 Implementation

The time step selection method is coded directly into the Serpent 2 code. The development within a reactor physics code is advantageous by allowing the method to be tested directly within the reactor analysis environment. The optimal procedure is to provide multiple fitted regimes with separate constants. This means that the method should be split to allow for fitting to the varying behaviors seen in figure 2.21. The fitting constants attempt to account for the changes in the system behavior and therefore acts as importances on the derived parameters. This approach enhances the adaptive behavior without introducing further computational burden. It is not known whether this process can be applied ubiquitously to other reactor systems.

The resulting segmentation of the time step selection function is formulated to isolate region 5 during the computation by using thresholds on the dk_p and $sR_a(t)$ functions as follows:

$$(dk_p \leq 1 \times 10^{-5} \text{ and } sR_a(t) > 0.008) \tag{3.1}$$

The selection of this region is based on the available parameters from the derivation. There are no other consistent formulations, with the reference cases, that permit further segmentation.

The result of the updateTimeStep() function is the new time step. There are other checks which might be required. These are not discussed since they are specific to the reactor physics code; for example, it might be necessary to check the time step in order ensure it does not exceed the desired burnup. The resulting time step is used to update the EOS isotopics prior to the corrector transport calculation. More advanced time integrations methods could potentially be used by altering the coefficients; however, this extension is not addressed in this dissertation.

The following pseudo-code describes the work flow for updateTimeStep() within the Serpent 2 code:

$h = initialTimestep$

$h_{max} = maxStepsize$

updateTimeStep()

if $(dk_p \leq 1 \times 10^{-5}$ and $sR_a(t) > 0.008)$

set $Constants = D_1, D_2, D_3, D_4, D_5$

else

set $Constants = C_1, C_2, C_3, C_4, C_5$

solve if $(dk_p > 0)\{p_1 = C_1 dk_p\}$; else $\{p_1 = 0\}$;

solve $p2 = C_2 \left(\frac{fR_a(t_o)}{fR_a(0)}\right)^{C_3} \left(\frac{f_a(t_1)}{f_a(0)}\right)^{C_4} \left(\frac{k_p(t_o)}{k_p(0)}\right)$

solve $p3 = C_5 \left[1 - \left(\frac{R_a(t_1)}{R_a(0)} \frac{f_a(t_1)}{f_a(0)}\right)\right]$

$h = initialTimestep \times (p_3(p_1 + 1) + p_2)$

if $h > h_{max}\{h = h_{max}\}$

return h

The constant coefficients are determined using a linear, least-squares regression on the temporally converged solutions, noting that there are two sets of constants given by the function condition for region 5, which states:

$$Constants = \begin{cases} D_x & \text{for } dk_p(t) \leq 1 \times 10^{-5} \text{ and } sR_a(t) > 0.008, \quad (3.2) \\ C_x & \text{else.} \quad (3.3) \end{cases}$$

where x is the coefficient index. A small value of $1e-5$ is used instead of 0 for the constant selection, simply to protect the threshold evaluation from any round-off error. The 0.008 value comes from the asymptotic behavior in the $sR_a(t)$ function. This is expected to be dependent on the system depletion rate and overall behavior resulting from, for example, a graphite moderated or sodium fast reactor. Therefore, care should be taken to address whether this parameter is suitable for other systems.

The fit produced for the LWR system under consideration determines the constant values by assessing the error on the time step size predicted from the method to the time step sizes necessary for a temporally converged result determined in section 2. The optimized constants reduce the error between these solutions. The resulting coefficients, determined by applying a least squares fit to all of the cases, are:

$$D_1 = \ , D_2 = 0.6959, D_3 = -3.1402, D_4 = -3.0252, D_5 = -9.2646$$

$$C_1 = 24.6397, C_2 = 0.1260, C_3 = 0.7273, C_4 = -1.1264, C_5 = 0.0245$$

where the D_1 coefficient is not necessary. The parameter which D_1 is multiplied to is equal to zero for the following conditions: $dk_p(t) \leq 1 \times 10^{-5}$ and $sR_a(t) > 0.008$, as seen in figure 2.23.

If an initial step size of 1 $\frac{MWd}{kg}$ is used along with the aforementioned coefficients, the updated time steps can be determined. These are shown in figure 3.1 for each of the cases. Comparing this figure to that of figure 2.19, it is immediately noticed

that the BOL performance of nozones and noBAs is poorly predicted. The behavior, however, of the other cases is reasonable, though not ideal. The expected time step selection, from this figure, indicate that the computational burden will be greater than needed for a temporally converged solution.

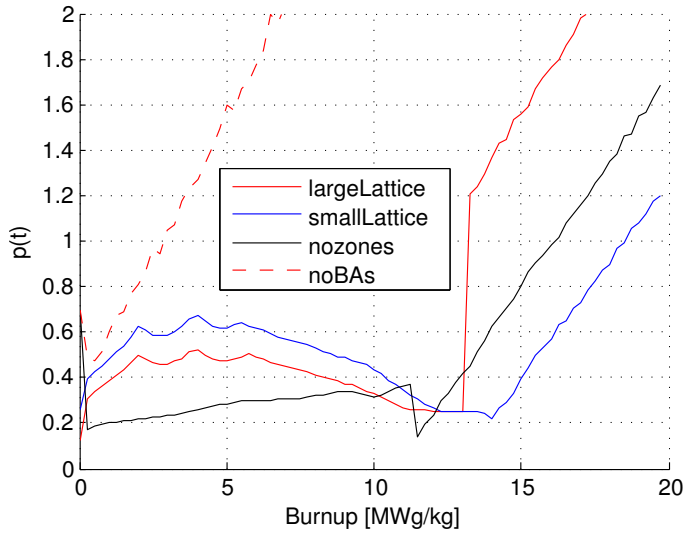

Figure 3.1: Updated time steps as a function of burnup.

3.2 Demonstration

This method is demonstrated on the four cases evaluated in the previous section. For the method to be successful, the solution should approach the converged solution with a minimal increase in computational effort. In other words, the errors in the multiplication factor, nuclide densities, and reaction rates, should be small; however, unlike in the previous evaluation, the direct comparison at each successive level of refinement is not possible. The same temporal grid is not used with the developed approach. This is because this methodology is stochastic in nature as it depends on the reaction rates determined during the Monte Carlo neutron transport simulation.

Therefore, there will be additional error introduced when interpolating between time steps to compare the solutions.

The method is applied to the previous cases. The time steps resulting from the simulations are shown in figure 3.2 for all of the cases.

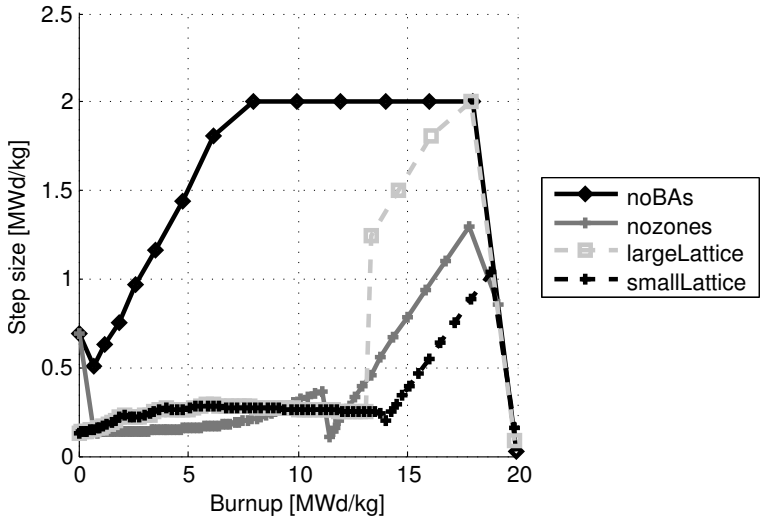

Figure 3.2: Time step from method as a function of burnup.

In figure 3.3, the time steps from the methodology is compared to the time steps from the resolved cases. This shows the results from the method (solid line) compared to the time steps from the manual refinement (figure 2.19). The method mostly exhibits the appropriate behavior, noting that the sharp tail at the end of the depletion is the adjustment of the last step to meet the input depletion of 20 $\frac{MWd}{kg}$.

However, there are a few regions which are not predicted very well. In particular, the method does not refine the initial irradiation and resulting production of fission products in the fresh fuel, region 1, for the nozones and noBAs cases. This is arguably the most important region to refine due to explicit time nature of the solution. An

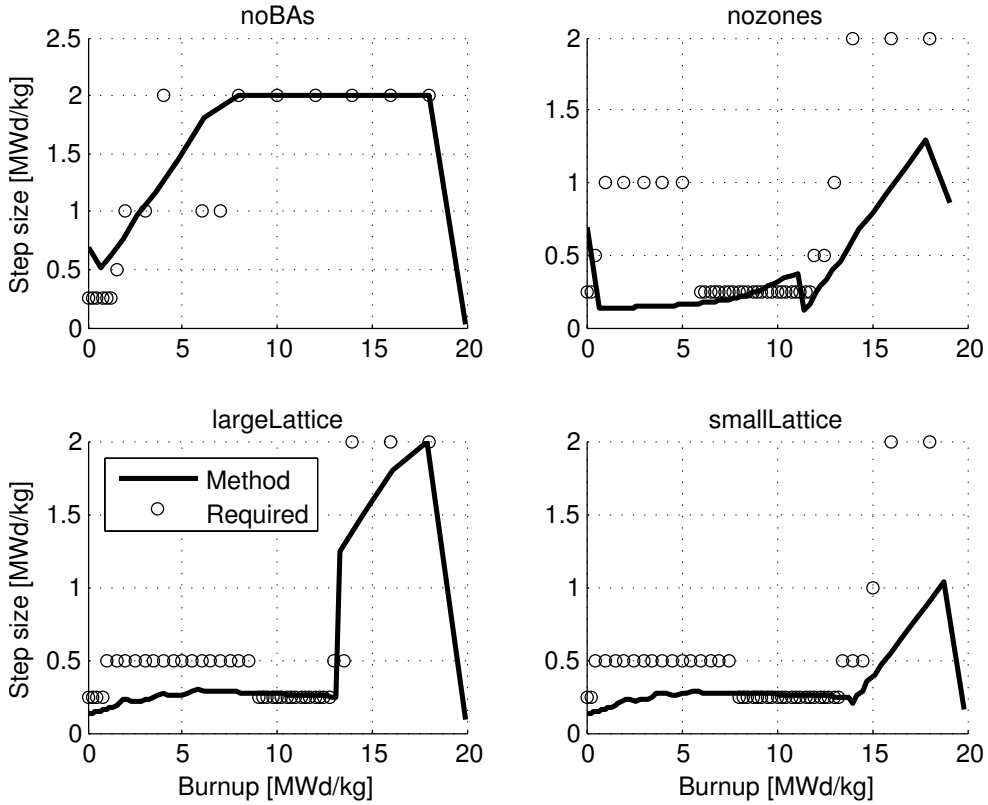

Figure 3.3: Comparison of time step as a function of burnup.

additional "if" statement will be necessary for expanding this methodology to these kinds of cases. The refinement for the largeLattice and smallLattice cases is more than necessary, reducing the computational effectiveness of the method; however, the behavior is sufficient to provide a close-to-converged solution.

3.2.1 Verification

The solution produced by the adaptive temporal method in the previous section is checked for a temporally converged solution. This verification is performed by manually refining the time steps uniformly, and evaluating the resulting errors on the eigenvalue and the nuclide densities similarly to the study performed in section 2.

The eigenvalue is shown in figure 3.4 and the resulting error, in pcm, by increasing the level pf refinement is shown in figure 3.5 for each case.

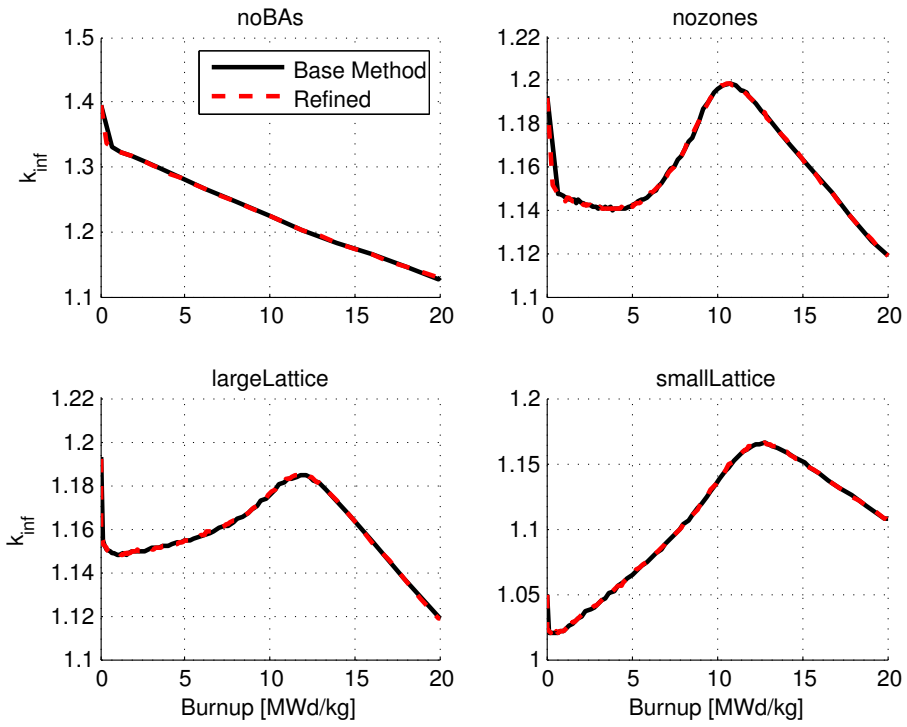

Figure 3.4: Infinite eigenvalue as a function of burnup for each case using the adaptive method.

This shows that the method ensures that the time step size is sufficient and adequate to capture the excess reactivity change with burnup without necessitating further refinement in time. The resulting errors are in fact dominated by the statistical errors. For these simulations, the statistical convergence was modest to allow for timely simulations. This does not impact that validity of the method demonstration.

The nuclide densities for select nuclides and the resulting error is shown in figures 3.6, 3.7, 3.8, and 3.9, for the noBAs, nozones, largeLattice, and smallLattice cases, respectively.

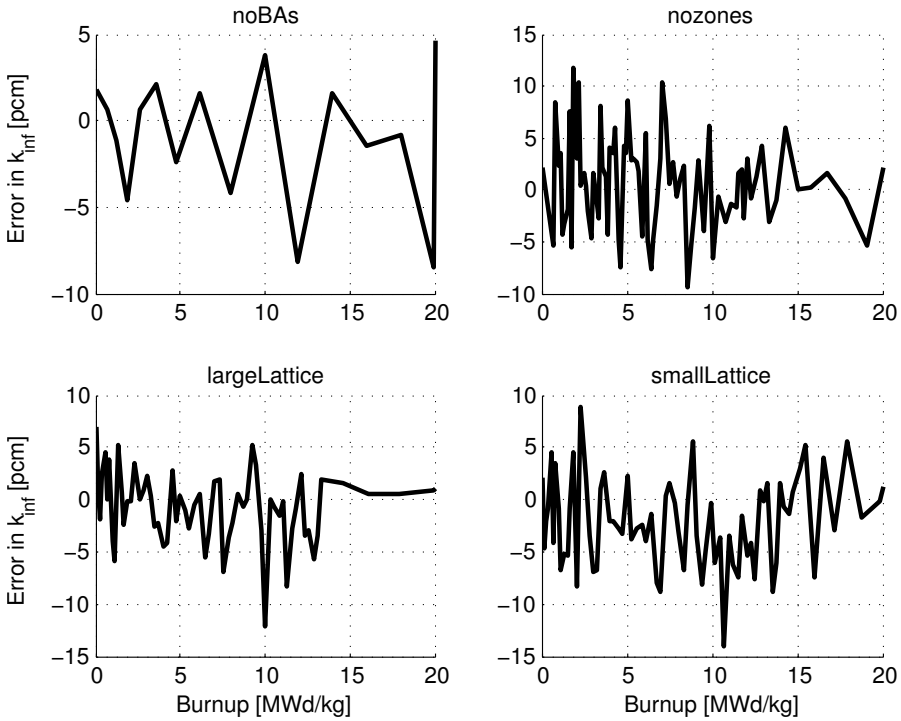

Figure 3.5: Error of infinite eigenvalue as a function of burnup for each case comparing the adaptive method to a more highly refined solution.

The results above demonstrate an excellent prediction of the necessary time steps to ensure a close-to-converged solution for all of the cases. There are, as expected, some systematic errors; however, the maximum errors in the nuclide density is typically less that 2 percent.

3.2.2 Discussion

The method has been demonstrated by implementing the method in the Serpent 2 reactor physics code. This provides a sound foundation to test the method with typical reactor physics problems. The developed method was demonstrated to appropriately select the next time step of a depletion sequence during the predictor step. This approach ensures a minimal computational cost.

A verification study was performed to ensure that the solution was close to con-

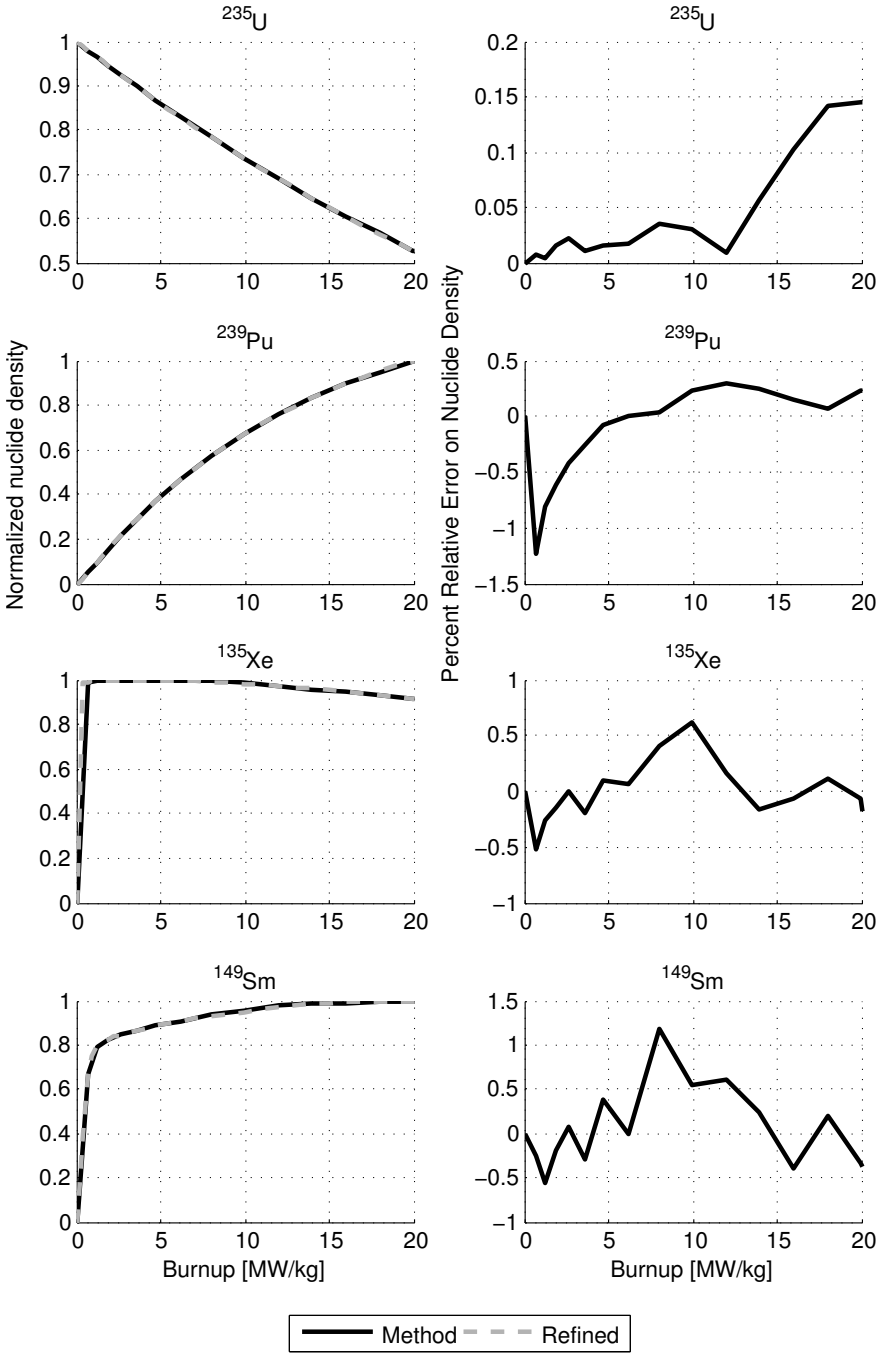

Figure 3.6: Nuclide densities for select nuclides as a function of burnup for noBAs case.

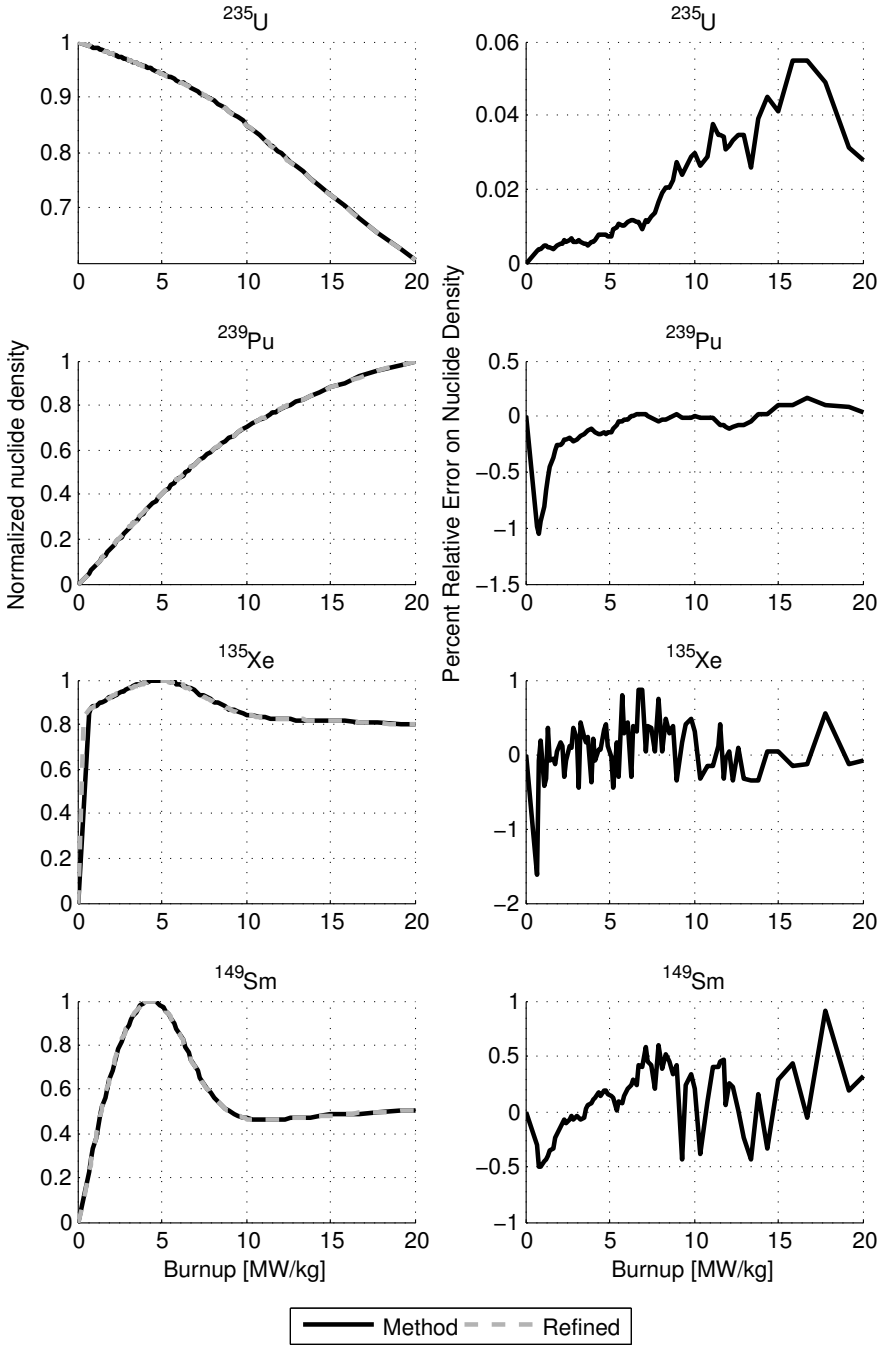

Figure 3.7: Nuclide densities for select nuclides as a function of burnup for nozones case.

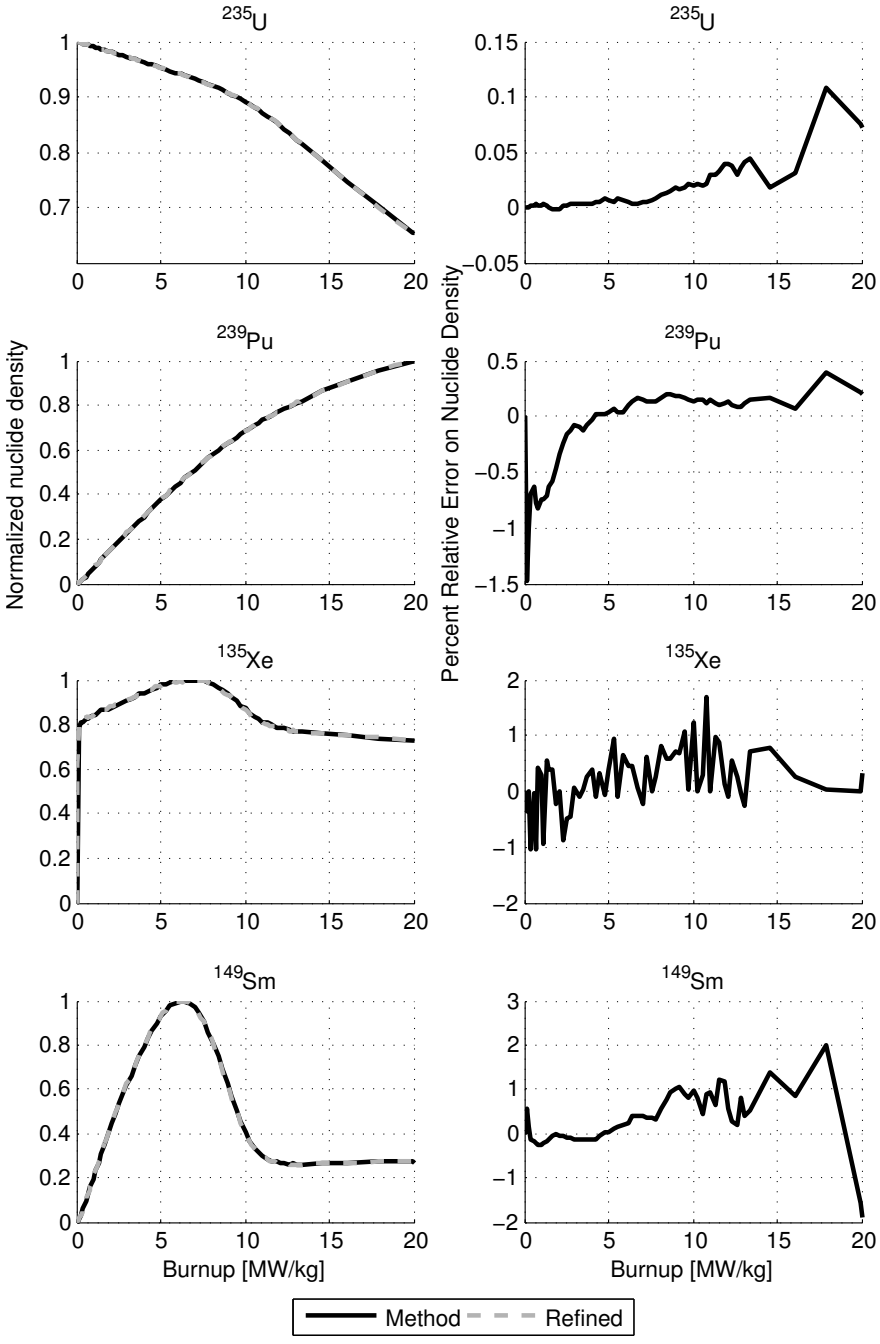

Figure 3.8: Nuclide densities for select nuclides as a function of burnup for largeLattice case.

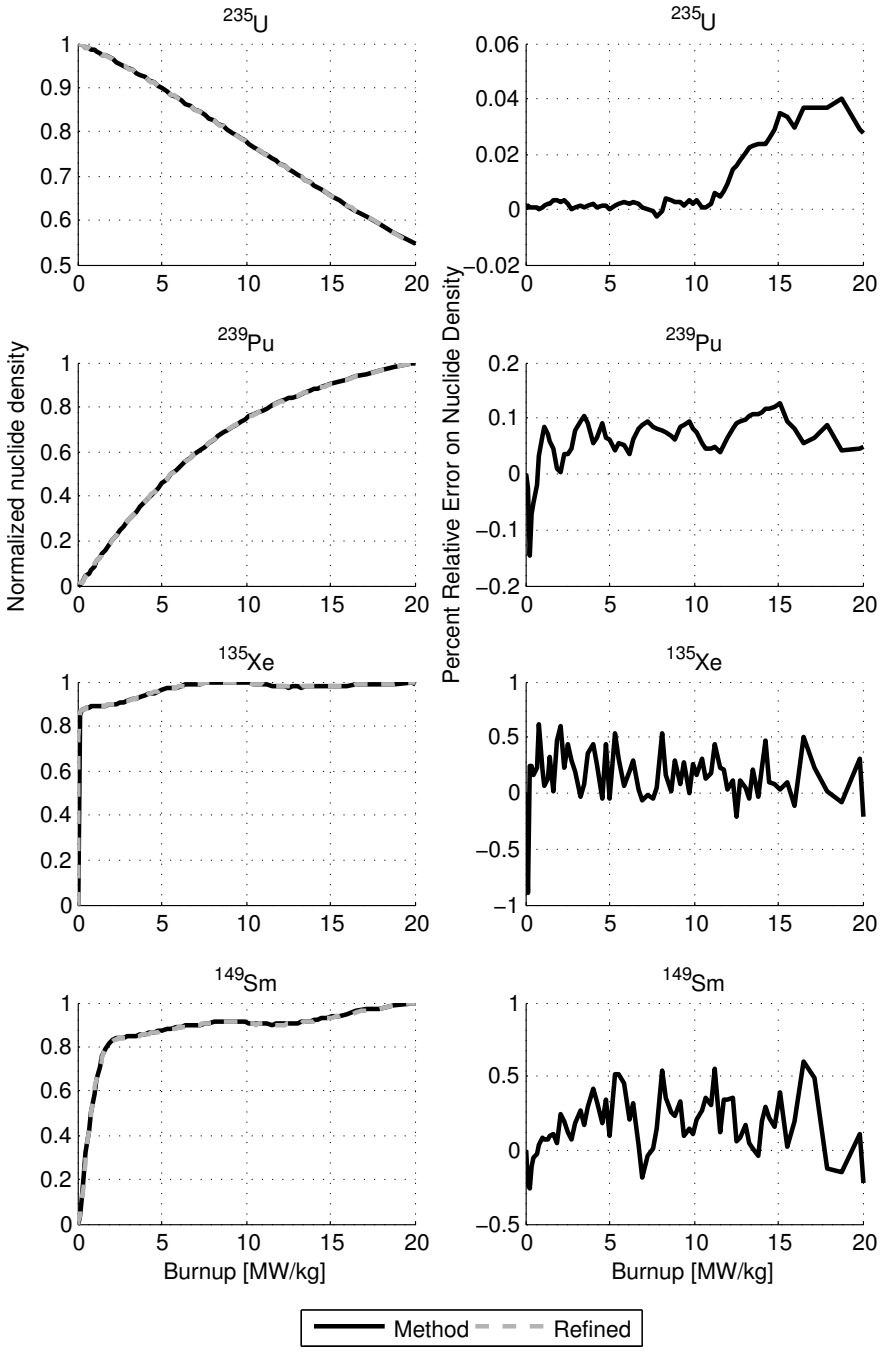

Figure 3.9: Nuclide densities for select nuclides as a function of burnup for smallLattice case.

vergence. This is a necessary condition for this method to be useful. The eigenvalue and nuclide density were satisfactorily computed as a function of burnup with small temporal errors of less than 14 pcm for the multiplication factor and less than 2 percent for the nuclide densities. The behavior of the error suggests that a majority of the error is statistical in nature and not systematic.

Overall, the method appears to be effective at providing an automated, predictive time-steps for depletion coupled neutron transport simulations. As a consequence of its derivation, there are constants that must be determined by fitting to existing, similar cases. It is not known if these can be used universally for other, vastly different systems. There are a number of assumptions that have gone into this development. These will be enumerated in the next section.

3.3 Summary

A novel method for a dynamic, predictive, and physics-based time step selection for coupled neutron transport and depletion simulations has been developed and was demonstrated to effectively predict the necessary time steps to ensure a close-to-converged solution. This method was implemented directly within the Serpent 2 reactor physics code and a verification study was completed to ensure satisfactory temporally converged solutions compared to user specified time steps in four reference cases.

There are some known and suspected limitations of the method, given the assumptions used during its development. Foremost, the method makes use of the reaction rates determined by the neutron transport. This results in computation of step size that is subjected to statistical noise from the Monte Carlo method. This results in simulations that have some randomness to the time step discretization. The impact is expected to be minor; however, the user must be aware of this effect.

The method was not tested for large systems that exhibit loose spatial coupling. This kind of coupling is prominent in systems where the neutron mean-free path length is small compared to the reactor geometry, particularly in full-core simulations. This added dimensionality was ignored in the analysis by using a 2D infinite lattice. Thorough testing is necessary if this method is to be expanded to larger systems.

The only system analyzed was the pressurized light water reactor. This type of system is characterized by a thermal neutron spectrum and small pin diameters compared to the neutron mean-free path length. The cases analyzed vary only slightly from this configuration, such as removing or including Gd_2O3 burnable absorber rods. The impact of self-shielding was also addressed. This leaves a great number of systems untested and requiring further study.

Transient cases were not tested with this algorithm. It is unknown if power changes during burnup will be appropriately refined to capture equilibrium changes in the fission product inventories.

Further improvements of the method might include previous time step information. For example, the previous step's corrector neutron flux and nuclide distribution may contain useful information on how the coupled sequence is behaving. The disparity between the current step predictor and the previous step corrector solutions may provide added information for determining the time step size. This was not addressed in this dissertation.

This dissertation has outlined a number of difficulties that arise from the coupled neutron transport and depletion simulations. In particular, a thorough analysis of the temporal convergence problem was performed for a number of light water reactor type, 2D, infinite lattice calculations. The time step requirements were determined manually using a system that was determined to be numerically stable and statistically converged.

This process of manually specifying time steps and assessing whether the temporal solution is converged or not is the typical procedure for coupled simulations. However, this can be very costly, requiring many simulations to be performed. Often this procedure is not preformed in many analyses. The time step selection process is often performed with a priori knowledge of the system behavior and understanding of the physics complexity which arises from the tightness of coupling between various phenomena. Scoping analyses can be performed to investigate whether increased temporal resolution is necessary; however, repeating many complex and large Monte Carlo simulations is often particularly prohibitive.

This method was developed to assist in addressing this temporal convergence issue by providing an in situ, predictive estimate of the time steps during the depletion calculation. This type of approach has numerous advantages. Such a method preferentially frees the reactor designer from performing numerous simulations by reducing the burden of having to perform many coupled neutron transport and depletion simulation to ensure temporal convergence. Ideally, such a method addresses general system analysis without increasing the computational requirements significantly. Unlike in the traditional sense of adaptive methods, this methods performs a predictive time step selection without iterating over the solution, thereby saving significant computational effort.

REFERENCES

[1] S. Agostinelli and et al. Geant4âĂŤa simulation toolkit. *Nuclear Instruments and Methods in Physics Research Section A: Accelerators, Spectrometers, Detectors and Associated Equipment* , 506(3):250 – 303, 2003.

[2] K. Binder. *Applications of the Monte Carlo Method in Statistical Physics*. Springer-Verlag, 1987.

[3] F. B. Brown. MCNPâĂŞA General Monte Carlo NâĂŞParticle Transport Code, Version 5 Overview and Theory. Technical report, Los Alamos National Laboratory, 2003.

[4] E. Brun, E. Dumonteil, and F. Malvagi. Systematic Uncertainty Due to Statistics in Monte Carlo Burnup Codes: Application to a Simple Benchmark with TRIPOLI-4-D. *Progress in Nuclear Science and Technology*, 2:879–885, 2011.

[5] Y. Cao, Y. Gohar, and C. H. M. Broeders. MCNPX Monte Carlo burnup simulations of the isotope correlation experiments in the NPP Obrigheim. *Annals of Nuclear Energy*, 37:1321–1328, 2010.

[6] J. Cetnar. General solution of Bateman equations for nuclear transmutations. *Annals of Nuclear Energy*, 33:640–645, 2006.

[7] M. B Chadwick and et al. ENDF/B-VII.1 Nuclear Data for Science and Technology: Cross-Sections, Covariances, Fission Product Yields and Decay Data. Technical report, Nucl. Data Sheets 112, 2011.

[8] J. Concato. Monte Carlo Methods in Clinical Research: Applications in Multivariable Analysis. *Journal of investigative medicine*, pages 394–400, 1997.

[9] D. E. Cullen. TART2012: An Overview of A Coupled Neutron-Photon 3-D, Combinatorial Geometry, Time Dependent Monte Carlo Transport Code. Technical report, Lawrence Livermore National Laboratory, 2012.

[10] J. Dufek and J. Hoogenboom. Numerical stability of Existing Monte Carlo Burnup Codes in Cycle Calculations of Critical Reactors. *Nuclear Science and Engineering*, 162:307–311, 2009.

[11] J. Dufek, D. Kotlyar, and E. Shwageraus. The stochastic implicit Euler method - A stable coupling scheme for Monte Carlo burnup calculations. *Annals of Nuclear Energy*, 60:295–300, 2013.

[12] J. Dufek, D. Kotlyar, E. Shwageraus, and J. Leppänen. Numerical stability of the predictor-corrector method in monte carlo burnup calculations of critical reactors. *Annals of Nuclear Energy*, 56:34–38, 2013.

[13] J. Dufek and V. Valtavirta. Time step length versus efficiency of Monte Carlo burnup calculations. *Annals of Nuclear Energy*, 72:409–412, 2014.

[14] N. Garcia-Herranz, O. Cabellos, J. Sanz, J. Juan, and J. C. Kuijper. Propagation of statistical and nuclear data uncertainties in Monte Carlo burn-up calculations. *Annals of Nuclear Energy*, 35:714–730, 2008.

[15] D. P. Greisheimer and et al. MC21 v.6.0 - A Continuous-Energy Monte Carlo Particle Transport Code with Integrated Reactor Feedback Capabilities. *Joint International Conference on Supercomputing in Nuclear Applications and Monte Carlo 2013*, 2013.

[16] R. L. Harrison. Introduction to Monte Carlo Simulation. In *AIP Conf Proc.*, January 2010.

[17] G. IIas, I. C. Gauld, F. C. Difilippo, and M. B. Emmett. Analysis of Experimental Data for High Burnup PWR Spent Fuel Isotopic Validation - Calvert Cliffs, Takahama, and Three Mile Island Reactors. Technical report, Oak Ridge National Laboratory, 2010.

[18] A. Isotalo. *Computational methods for burnup calculations with Monte Carlo neutronics*. PhD thesis, Aalto University, 2013.

[19] A. Isotalo and P. Aarnio. Higher order method for burnup calculations with Bateman solutions. *Ann. Nucl. Energy*, 38:1987–1995, 2011.

[20] A. E. Isotalo and P. A. Aarnio. Substep methods for burnup calculations with Bateman solutions. *Annals of Nuclear Energy*, 38:2509–2514, 2011.

[21] S. Kalchezva and E. Koonen. Automatic Whole Core Depletion & Criticality Calculations by MCNPX 2.7.0. In *PHYSOR*, 2012.

[22] D. Kelly, T. Sutton, and S. Wilson. MC21 Analysis of the Nuclear Energy Agency Monte Carlo Performance Benchmark Problem. In *PHYSOR*, 2012.

[23] D. Kotlyar and E. Shwageraus. On the use of predictor-corrector method of coupled monte carlo burnup codes. *Annals of Nuclear Energy*, 58:228–237, 2013.

[24] J. Leppänen. *Development of a new Monte Carlo reactor physics code*. PhD thesis, Helsinki University of Technology, 2007.

[25] J. Leppänen. Performance of Woodcock delta-tracking in lattice physics applications using the Serpent Monte Carlo reactor physics burnup calculation code. *Ann. Nucl. Energy*, 37:715–722, 2010.

[26] J. Leppänen. Serpent - a Continuous-energy Monte Carlo Reactor Physics Burnup Calculation Code. User's Manual. *VTT Technical Research Centre of Finland*, March 2013.

[27] J. LeppÃđnen and A. Isotalo. Burnup calculation methodology in the Serpent 2 Monte Carlo code. In *PHYSOR*, 2012.

[28] G. Marleau, A. Hebert, and R. Roy. A User Guide for DRAGON. Version DRAGON Release 3.04. Technical report, Institut de genie nucleaire, ÃĽcole Polytechnique de Montreal, 2000.

[29] M. Mascagni. Monte Carlo Methods: Early History and the Basics. Technical report, Florida State University, 2011.

[30] N. Metropolis. The Beginning of the Monte Carlo Method. *Los Alamos Science*, Special Issue, 1987.

[31] Y. Nakahara, K. Suyama, and T. Suzaki. Translation of Technical Development on Burn-up Credit For Spent LWR Fuels. Technical report, Oak Ridge National Laboratory, 2002.

[32] M. Pusa. *Numerical methods for nuclear fuel burnup calculations*. PhD thesis, Aalto University, 2013.

[33] P. K. Romano and B. Forget. The OpenMC Monte Carlo particle transport code. *Annals of Nuclear Energy*, 51:274 – 281, 2013.

[34] A. Santamerina and et al. The JEFF-3.1.1 Nuclear Data Library. Technical report, OECD NEA, 2009.

[35] J. Spanier and E. M. Gelbard. *Monte Carlo Principles and Neutron Transport Problems*. Dover Publications, 2008.

[36] M. Tohjoh, T. Endo, M. Watanabe, and A. Yamamoto. Effect of error propagation of nuclide number densities on Monte Carlo burn-up calculations. *Annals of Nuclear Energy*, 33:1424–1436, 2006.